感知毫微微蜂巢網路中
基於低複雜度合作頻譜感測之分散式頻譜存取

學生：李慎中　　　　　　　指導教授：李大嵩 博士

國立交通大學電信工程研究所碩士班

摘要

　　於本研究中，吾人提出一種適用於感知毫微微蜂巢網路中(cognitive femtocell network)基於頻譜感測資訊之頻譜配置法。此方法可在頻譜隱匿式及頻譜重疊式之混合策略下(joint spectrum overlay and underlay strategy)有效增加頻譜重覆使用率。吾人首先將頻譜配置的問題轉化成一個非合作式賽局的形式，並且使用賽局理論中的遺憾匹配學習演算法(regret-matching learning algorithm)來獲得最佳解。為了得到在頻譜配置時需要的相關感測資訊，吾人提出一種基於最大最小特徵值(maximum-minimum eigenvalue; MME)感測技術的新式合作頻譜感測法，在提出的方法中，基地台間可利用廣播的方式與鄰近基地台交換特徵值的資訊，以達到合作的目的並增進感測效能。這種新的合作方式使得基地台在交換訊息時有著較小的傳輸負擔以及較少的運算複雜度。最後，電腦模擬結果顯示出吾人提出的新式的合作頻譜感測法可以達到和傳統的方法幾乎相同的效能，以及吾人提出的基於頻譜感測資訊之頻譜資源配置法，可在頻譜隱匿式及頻譜重疊式之混合策略下有效增加頻譜重覆使用率。

Distributed Spectrum Access with Low Complexity Cooperative Sensing in Cognitive Femtocell Networks

Student: Shen-Chung Lee   Advisor: Dr. Ta-Sung Lee

Institute of Communications Engineering
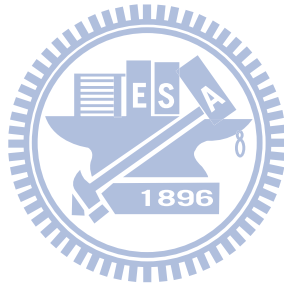
National Chiao Tung University

Abstract

In this thesis, we develop a sensing-based spectrum allocation scheme with joint spectrum overlay and underlay strategy to increase the frequency reuse factor among cognitive femtocell networks. The spectrum allocation problem is firstly formulated as a non-cooperative game and the regret-matching learning algorithm in game theory is used to solve the problem. To obtain the sensing-based information for spectrum allocation, a new maximum-minimum eigenvalue-based (MME-based) cooperative sensing scheme is proposed which shares the information of eigenvalues with neighboring femtocells via wireless broadcasting to enhance detection probability in cognitive femtocell networks. The new cooperative scheme uses a small overhead for exchanging local information and requires a low complexity for local computations. Finally, computer simulation results show that the new spectrum sensing scheme can achieve nearly the same sensing performance as conventional methods and the proposed sensing-based spectrum allocation scheme with joint spectrum overlay and underlay strategy can increase the frequency reuse factor effectively.

Acknowledgement

Table of Contents

List of Figures

List of Tables

Acronym Glossary

AWGN   additive white Gaussian noise

CDF   cumulative distribution function

CR   cognitive radio

EVD   eigenvalue decomposition

FAP   femtocell access point

FUE   femtocell user equipment

F_{TW2} CDF of Tracy-Widom distribution of order two

IEEE   institute of electrical and electronics engineers

LTE   long term evolution

MBS   macrocell base station

MIMO   multiple-input multiple-output

MUE   macrocell user equipment

MME   maximum-minimum eigenvalue

NU   noise uncertainty

OFDMA   orthogonal frequency division multiple access

PDF   probability density function

PU   primary user

RB   resource block

RI   reliability indicator

SNR   signal-to-noise ratio

SON   self-organizing network

SU   secondary user

TW_2 Tracy-Widom distribution of order two
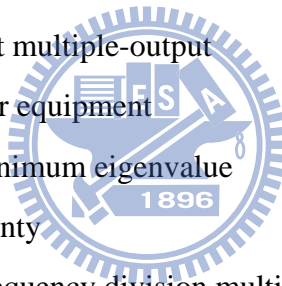
Notations

$\mathcal{A}$	joint actions space of K FAPs
$\mathcal{A}_k$	action space of the kth FAP
$\mathbf{a}_k^t$	action taken by the kth FAP at time instant t
$\mathbf{a}_{-k}^t$	action of all players except the kth player at time instant t
D	number of maximum and minimum eigenvalues used in the proposed method
$\mathbf{G}_k(\mathbf{p}^t)$	instantaneous regret matrix of the kth FAP at time instant t
$\mathcal{H}_0 / \mathcal{H}_1$	PUs' signal is absent/present
$\mathbf{H}$	channel matrix
$h_{m,p}$	channel effects between PUs and SUs
$I_{ff,k}^{\ t}(f)$	co-tier interference at time instant t
$I_{mf,k}^{\ t}(f)$	cross-tier interference at time instant t
K	number of FAPs in the same cluster
L	observation window size
M	number of FAP's antennas
N	number of channel tapes
N_s	number of samples
N_{mul}	number of multiplications
N_{add}	number of additions
N_{RB}	total number of RBs
N_{MUE}	number of MUEs
N_{idle}	number of idle RBs which are unoccupied by MUEs
$N_{aRB,1} / N_{aRB,2}$	number of avaliable RBs with /without cross-tier interference
N_{aRB}	total number of avaliable RBs
P	number of primary users
P_{fa}	probability of false alarm
P_d	probability of detection

$\mathbf{R}_Y$	covariance matrix of FAP received signal vector
$\mathbf{R}_V$	covariance matrix of noise vector
$\mathbf{R}_S$	covariance matrix of primary signal vector
RI	reliability indicator
S_j / S_i	current/next action playing by FAPs
T	test statistic of MME detector
U_k^t	local utility function of FAP k at time instant t
$v_m(n)\}$	complex Gaussian noise $\sim CN\left(0, \sigma_v^2\right)$
$\boldsymbol{V}(n)$	complex Gaussian noise $\sim CN\left(\mathbf{0}, \sigma_v^2\mathbf{I}\right)$
$\mathbf{X}(n)$	primary user signal at the nth sample
$x_p(n)$	the pth PU signal at the nth sample
$\mathbf{Y}(n)$	sampled signal at the receiver at the nth sample
$\mathbf{y}(n)$	vector sampled by the M antennas at an FAP at the nth sample
$y_m(n)$	received signal from an N-tap channel at the mth antenna
α	noise uncertainty factor
γ	preset threshold to detect the presence of PUs
ε^t	decreasing step size at time t
η	suppressing factor
$\boldsymbol{\theta}_k^t$	overall regret matrix of the kth FAP at time t
λ_j	eigenvalue of received signal covariance matrix
μ	the constant used in regret-matching algorithm to ensure that the probability is non-negative
ρ_j	eigenvalue of primary signal covariance matrix
σ_j	eigenvalue of noise covariance matrix

Chapter 1

Introduction

In the rapid deployment of next-generation wireless communication applications, demands on spectrum have dramatically increased and traditional strategy of fixed spectrum assignment is inefficient. Therefore, the efficiency of spectrum utilization has become an important issue. A flexible way of available spectrum utilization, known as dynamic spectrum access, introduces the idea of Cognitive Radio (CR) [1]. CR is a technique that allows the so-called "secondary users (SUs)" to use unused bands on the premise of not affecting "primary users (PUs)". The concept of CR has been introduced in the deployment of femtocell networks [2].

The CR-based femtocell is a useful technique for increasing the frequency reuse factor and meeting a variety of service requirements. Femtocells can be classified as open or closed access [3]. The closed access deployment is considered in this work, i.e. the closed access deployment only permits each user to link with its served femtocell. Since a femtocell act as an SU, the mitigation of interference between PUs and SUs becomes an important issue [4]. Moreover, because the femtocell is an undefined and user-plug-in system, its self-organizing network (SON) [5] capability is of vital importance. To reach the goal of reusing spectrum resource, the following two

functionalities of the CR-based femtocell are needed:

- **Cooperative spectrum sensing:**

    CR networks need to sense the radio bands in the nearby environment to detect spectrum holes and estimate interference status. Some spectrum sensing algorithms have been proposed in [6]. An eigenvalue-based detection algorithm called maximum-minimum eigenvalue (MME) is proposed in [7], which exhibits advantages such as simultaneously achieving both high probability of detection and low probability of false alarm rate, resisted noise uncertainty [8], and without requiring information from primary signals and noise power. Furthermore, [9] derives the exact decision threshold of the MME method depending on probability of false alarm rate subject to the constraint of a finite number of cooperative receivers and samples.

    Since primary signals often need to penetrate walls and then be received by the femtocells, they may encounter serious shadowing and fading problems, causing that the SUs encounter a hidden PU problem. In this case, the cooperative methods could be employed to ensure the reliability of spectrum sensing detection [1]. Cooperative spectrum sensing schemes using eigenvalue-based technique have been discussed in [10]-[11]. In [10], the authors derive an analytic expression for the limiting eigenvalue ratio distribution, which turns out to be much more accurate than previous approximations. The authors of [11] propose a modified and improved MME method as reported in [7]. However, a stringent requirement of cooperative spectrum sensing is low amount of sensory data exchange and low computation complexity, because SU devices are usually low cost equipment [12]. To this end, we here propose a new approach of cooperative spectrum sensing based on the eigenvalue-based technique.

- **Spectrum allocation among femtocells:**

After the spectrum sensing phase, the problem that remains to be solved is spectrum allocation. A useful algorithm called the regret-matching algorithm in game theory can provide an effective way to solve such a competition problem in a distributed system, which has been proposed in [4], [13]-[16]. Regret- matching algorithm is a kind of learning algorithm, and its basic idea is to learn about the regret of its actions that had been taken at every time instant and aim at minimizing its regret value [17] [18].

In a game form, the femtocells act as the players and their actions are the selection of the new frequency band. In [13], the authors consider the downlink spectrum allocation problem with a pure overlay spectrum access strategy and design the local utility function incorporating self-interest, fairness and power consumption. Furthermore, [15] designs the actions with joint spectrum and power allocation and therefore the action space become larger. The authors of [16] show that the regret-matching learning algorithm has a similar performance with the potential game (potential game needs higher overhead for information exchange; in contrast, regret-matching algorithm does not exchange any information with other players). In practice, the pure overlay strategy is inefficient because of the demand of spectrum have dramatically increased in the cellular systems. Similar to the requirements mentioned in the cooperative spectrum sensing phase, we also require low amount of data exchange and low computational complexity in the spectrum allocation phase. To this end, we here propose a new approach of the game-theoretic spectrum allocation based on the spectrum sensing information.

In this thesis, we develop a sensing-based spectrum allocation scheme with joint spectrum overlay and underlay strategy to solve the insufficient spectrum resource problem. To obtain the sensing-based information, we also develop a low exchange overhead and low computational complexity decentralized cooperative spectrum sensing scheme which shares the information of eigenvalues with neighboring femtocells to obtain a new test statistic via wireless broadcasting. The exchange overhead and local computation complexity of the proposed scheme will be analyzed.

The remainder of this thesis is organized as follows. Chapter 2 introduces the general scenario and the conventional MME-based cooperative spectrum sensing scheme. A new MME-based cooperative spectrum sensing scheme which employs cluster-based information exchange to obtain a new test statistic is presented in Chapter 3. In Chapter 4, the spectrum allocation problem among femtocells with joint spectrum overlay and underlay strategy is solved with game theory. Finally, Chapter 5 gives the conclusions and the future works.

Chapter 2

System Model

In this chapter, we consider the scenario depicted in Figure 2.1, in which a macrocell system coexist with a number of femtocell systems in an uplink OFDMA network. The basic frequency resource unit in our considered environment is called resource block (RB) and each RB is originally occupied by the macrocell system. Macrocell user equipments (MUEs) act as the PUs, who has the higher priority to access the licensed RBs, i.e. licensed uplink channel, and communicate with macro base station (MBS) via these RBs. In contrast, femtocell user equipments (FUEs) act as the SUs who
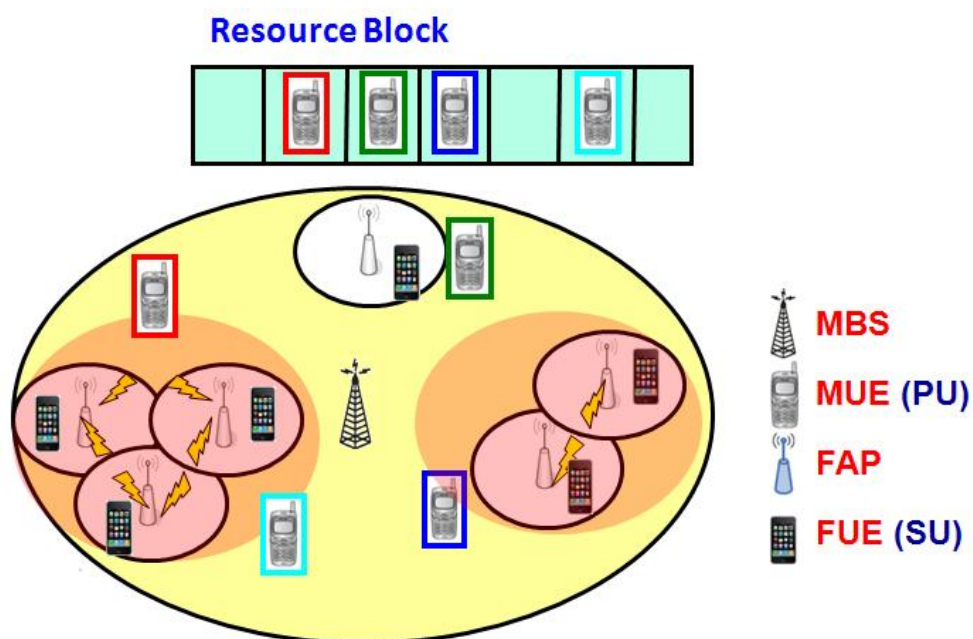
Figure 2.1: Coexistence of femtocell and macrocell system

only use the remaining RB linking with femtocell access points (FAPs) on the premise of not affecting PUs. To reach the purpose of not affecting PUs and reusing spectrum resource, the functionality of cooperative spectrum sensing is needed:

1. **Spectrum sensing**: FAPs should detect the presence of PUs and prevent the interference to macrocell system, and generate a link between FAP and corresponding served FUE using these available RBs for opportunistic transmissions.

2. **Cooperation**: although each FAP can do spectrum sensing individually, FAP can further do spectrum sensing jointly with other FAPs to avoid hidden node problem or a bad channel condition and improve the sensing reliability.

The remainder of this chapter is organized as follows. In Section 2.1, we will firstly present the system model for spectrum sensing. In Section 2.2, we compute the eigenvalues of covariance matrix of received signal vector and further analyze some characteristic of these eigenvalues. In Section 2.3, an introduction of a new spectrum sensing method called maximum minimum eigenvalue (MME) detection is presented. The traditional MME-based cooperative spectrum sensing method is introduced in Section 2.4. A summary of Chapter 2 is given in Section 2.5.

2.1 System Model

Spectrum sensing is a problem of detecting the primary signal and can be described as a binary hypothesis test as follows:

$$
\begin{aligned}
\mathcal{H}_0 : \ & \mathbf{Y}(n) = \mathbf{V}(n) \\
\mathcal{H}_1 : \ & \mathbf{Y}(n) = \mathbf{H} \cdot \mathbf{X}(n) + \mathbf{V}(n) \\
& = \mathbf{S}(n) + \mathbf{V}(n) \qquad , \ n = 1, 2, \ldots, N_s,
\end{aligned} \tag{2.1}
$$

where $\mathcal{H}_0$ and $\mathcal{H}_1$ denotes PUs' signal is absent or present. N_s is the sampled period and $\mathbf{Y}(n)$ denotes the sampled signal at the receiver at time instant n, $\mathbf{H}$ denotes the channel matrix including the multi-path fading and path loss effects, $\mathbf{X}(n)$ denotes the transmitted signal of the primary user and $\mathbf{V}(n)$ denotes the noise $\sim CN\left(\mathbf{0}, \sigma_v^2 \mathbf{I}\right)$. Moreover, there are two assumptions made in our system model:

1.　　Noise $\mathbf{V}(n)$ is independent of the primary signal $\mathbf{X}(n)$.

2.　　Channel effect matrix $\mathbf{H}$ is not a function of time, i.e. the channel effect between FAPs and MUEs are time-invariant during the sampled period.

Assume that each FAP is equipped with multi-antennas. Let $\mathbf{y}(n) = [y_1(n), y_2(n), \cdots, y_M(n)]^T$ be the vector sampled by the M antennas at an FAP at instant n, where $y_m(n)$ is the received signal from an N-tape channel at the mth antenna [7]:

$$
y_m(n) = \sum_{p=1}^{P} \sum_{g=1}^{N} h_{m,p}(g) x_p(n-g) + v_m(n), \ \ m = 1, \ldots, M \tag{2.2}
$$

where $\{x_p(n)\}$ are the PU signal, $\{h_{m,p}(n)\}$ are the corresponding channel effects between PUs and SUs, and $\{v_m(n)\}$ are the complex Gaussian noise $\sim CN\left(0, \sigma_v^2\right)$. For

detection performance consideration, it often requires to work with longer received observation vectors (the reason of which will be discussed in Section 2.3). To extend the length of the received observation vectors, we cascade delayed samples of $\mathbf{y}(n)$ into

$$\mathbf{Y}(n) = [\mathbf{y}(n)^T, \mathbf{y}(n-1)^T, \cdots, \mathbf{y}(n-(L-1))^T]^T , \quad n = 1, ..., N_S ,$$ illustrated in Figure 2.2. Every single point in Figure 2.2 stands for a vector $\mathbf{y}(n)$ with length M. The window covers L points corresponding to an aggregated sample and totally there are N_s such slides. This model can be put in matrix form below, in which every "$\mathbf{0}$" denotes a $M \times 1$ zero matrix, which is

$$
\begin{bmatrix} \mathbf{y}(n) \\ \mathbf{y}(n-1) \\ \vdots \\ \mathbf{y}(n-(L-1)) \end{bmatrix}_{ML \times 1} = \begin{bmatrix} \mathbf{H}_1 \mathbf{0} & \cdots & \mathbf{0} & \mathbf{H}_P \mathbf{0} & \cdots & \mathbf{0} \\ \mathbf{0}\,\mathbf{H}_1 & \cdots & \mathbf{0} & \mathbf{0}\,\mathbf{H}_P & \cdots & \mathbf{0} \\ \vdots & \ddots & \vdots & \vdots & \ddots & \vdots \\ \mathbf{0}\cdots & \mathbf{0} & \mathbf{H}_1 & \mathbf{0}\cdots & \mathbf{0} & \mathbf{H}_P \end{bmatrix}_{ML \times P(N+L-1)} \cdot \begin{bmatrix} \mathbf{x}_1(n) \\ \mathbf{x}_2(n) \\ \vdots \\ \mathbf{x}_P(n) \end{bmatrix}_{P(N+L-1)\times 1} + \mathbf{V}(n)_{ML\times 1} ,
$$

where $\mathbf{x}_p(n) = \left[x_p(n)^T, \cdots, x_p(n-(N+L-1))^T \right]^T_{(N+L)\times 1}$,

and $\mathbf{H}_p = \begin{bmatrix} h_{1,p}(1) & \cdots & h_{1,p}(N) \\ \vdots & \ddots & \vdots \\ h_{M,p}(1) & \cdots & h_{M,p}(N) \end{bmatrix}_{M \times N}$.

$$(2.3)$$
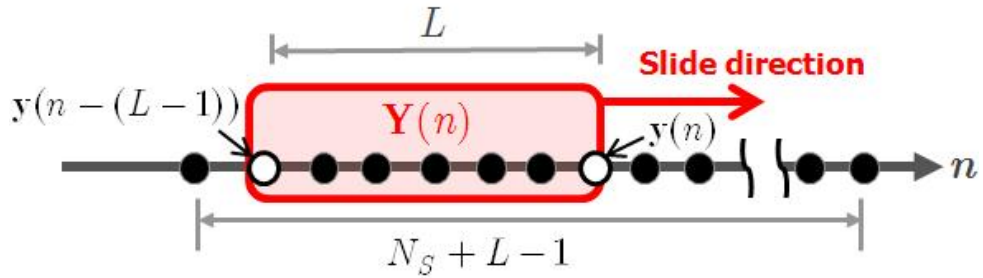
Figure 2.2: Illustration of received signal vector extension

2.2 Eigenvalue Analysis

1. Statistical covariance matrix:

Under $\mathcal{H}_1$, the statistical covariance matrix of the received signal $\mathbf{Y}(n)$ is derived as

$$
\begin{aligned}
\mathbf{R}_Y &= \mathrm{E}\left[\mathbf{Y} \cdot \mathbf{Y}^{\mathrm{H}}\right] = \mathrm{E}\left[(\mathbf{H} \cdot \mathbf{X} + \mathbf{V}) \cdot (\mathbf{H} \cdot \mathbf{X} + \mathbf{V})^{\mathrm{H}}\right] \\
&= \mathbf{H} \cdot \mathrm{E}\left[\cdot \mathbf{X} \cdot \mathbf{X}^{\mathrm{H}}\right] \cdot \mathbf{H}^{\mathrm{H}} + \mathrm{E}[\mathbf{V} \cdot \mathbf{V}^{\mathrm{H}}] \\
&= \mathbf{H} \cdot \mathbf{R}_{\mathrm{X}} \cdot \mathbf{H}^{\mathrm{H}} + \cdot\sigma_V^2 \cdot \mathbf{I}_{ML} \\
&= \mathbf{R}_S + \mathbf{R}_V .
\end{aligned}
\tag{2.4}
$$

where $\mathbf{R}_S$ and $\mathbf{R}_V$ denote the covariance matrices contributed by the primary signal and noise respectively. Under $\mathcal{H}_0$ condition, the received signal contains only the information of noise but not the primary signal. Lastly, $\mathbf{R}_Y$ equals $\mathbf{R}_V$ because $\mathbf{R}_S$ is absent.
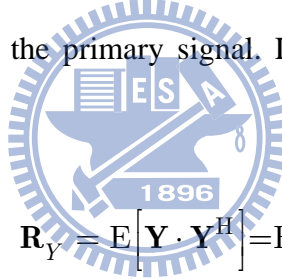
$$
\begin{aligned}
\mathbf{R}_Y &= \mathrm{E}\left[\mathbf{Y} \cdot \mathbf{Y}^{\mathrm{H}}\right] = \mathrm{E}[\mathbf{V} \cdot \mathbf{V}^{\mathrm{H}}] \\
&= \sigma_V^2 \cdot \mathbf{I}_{ML} \\
&= \mathbf{R}_V .
\end{aligned}
\tag{2.5}
$$

Performing eigenvalue decomposition (EVD) on $\mathbf{R}_S$ and $\mathbf{R}_V$, the corresponding eigenvalues are $\rho_1 > \rho_2 > ... > \rho_{ML}$ and $\sigma_1 = \sigma_2 = ... = \sigma_{ML} = \sigma_v$, and the eigenvalues of $\mathbf{R}_Y$ are $\lambda_1 > \lambda_2 > ... > \lambda_{ML}$, $\lambda_j = \rho_j + \sigma_j$, $j = 1, 2, ..., M \cdot L$. Intuitively, the presence of the primary signal has a strong effect on the composition of eigenvalues, thus it's a useful property for spectrum sensing and we will discuss it in detail in Section 2.3. Table 2.1 gives the summary of eigenvalues of the statistical covariance matrix both under $\mathcal{H}_0$ and $\mathcal{H}_1$.

Table 2.1: The summary of eigenvalues under $\mathcal{H}_0$ and $\mathcal{H}_1$

$\mathbf{R}_Y = \begin{cases} \mathbf{R}_V & ,\mathcal{H}_0 \\ \mathbf{R}_S + \mathbf{R}_V & ,\mathcal{H}_1 \end{cases} \Rightarrow \text{EVD}\{\mathbf{R}_Y\} = \begin{cases} \text{EVD}\{\mathbf{R}_V\} & ,\mathcal{H}_0 \\ \text{EVD}\{\mathbf{R}_S\} + \text{EVD}\{\mathbf{R}_V\} & ,\mathcal{H}_1 \end{cases}$	
$\text{EVD}\{\mathbf{R}_S\}$	$\rho_1 > \rho_2 > ... > \rho_{ML}$
$\text{EVD}\{\mathbf{R}_V\}$	$\sigma_1 = \sigma_2 = ... = \sigma_{ML} = \sigma_v$
$\text{EVD}\{\mathbf{R}_Y\}$	$\lambda_j = \rho_j + \sigma_j, \; j = 1,2,...,M \cdot L$ $\lambda_{\max} = \lambda_1 > \lambda_2 > ... > \lambda_{ML} = \lambda_{\min}$

It is worth mentioning that the number of non-zero eigenvalues of $\mathbf{R}_S$ depends on the rank of $\mathbf{R}_S$ and associated channel matrix $\mathbf{H}$. If the channel matrix $\mathbf{H}$ is of column full rank, i.e. $ML > P(N + L - 1)$, the last few eigenvalues will equal zeros.

2. N_s-sampled covariance matrix:

The statistical covariance matrix is not practical in digital computing. Thus we compute the N_s-sampled covariance matrix with N_s independent samples instead, which is

$$\mathbf{R}_Y(N_s) = \frac{1}{N_s}\left(\sum_{i=1}^{N_s} \mathbf{Y}(i) \cdot \mathbf{Y}^{\text{H}}(i)\right) = \frac{1}{N_s}\left(\mathbf{Y}_{N_s} \cdot \mathbf{Y}_{N_s}{}^{\text{H}}\right),$$

where

$$\mathbf{Y}_{N_s} = \begin{bmatrix} \mathbf{Y}(1) & \mathbf{Y}(2) & \cdots & \mathbf{Y}(N_s) \end{bmatrix}.$$

(2.6)

When the received signal is ergodic and $N_s \to \infty$, the N_s-sampled covariance matrix will approach the statistical covariance matrix. In practice, only a finite number of

samples are collected for $\mathbf{R}_Y(N_s)$ and the eigenvalues of $\mathbf{R}_V(N_s)$ would not be

$\sigma_1 = \sigma_2 = ... = \sigma_{ML} = \sigma_v$. Instead they would spread out and center around σ_v, i.e.,

$\sigma_1 \geq ... \geq \sigma_v \geq ... \geq \sigma_{ML}$. To better illustrate the property of eigenvalues, we give an

example ($M = 4$, $L = 1$, $P = 1$, $N = 1$, $\mathrm{SNR} = -5\mathrm{dB}$) which is shown in Table 2.2.

Under $\mathcal{H}_0$ condition, the eigenvalues are only contributed by the noise power, i.e.

$\lambda_j = \sigma_j$, $j = 1,2,...,M \cdot L$. In the case with $N_s = 30$, the differences between the

averaged eigenvalues are larger than the case with $N_s = 1000$. This is because too few

sample points are collected and therefore the N_s-sampled covariance matrix fails to

approach the statistical covariance matrix. Under $\mathcal{H}_1$ condition, the eigenvalues are

contributed both by the primary signal and noise power, i.e.

$\lambda_j = \rho_j + \sigma_j$, $j = 1,2,...,M \cdot L$. In this example, the size of the channel matrix $\mathbf{H}$ is

4×1, and channel matrix $\mathbf{H}$ is of column full rank. Hence, the number of non-zero

eigenvalues of $\mathbf{R}_S$ is also one. Eventually we can clearly observe that $E[\lambda_1]$ is much

larger than any averaged eigenvalues in Table 2.2.

Table 2.2: Averaged eigenvalues ($M = 4$, $L = 1$, $P = 1$, $N = 1$, $\mathrm{SNR} = -5\mathrm{dB}$)

		$E[\lambda_1]$	$E[\lambda_2]$	$E[\lambda_3]$	$E[\lambda_4]$
$N_s=30$	H_0	1.499	1.11	0.821	0.568
	H_1	2.468	1.273	0.907	0.617
$N_s=1000$	H_0	1.0810	1.0240	0.9741	0.9211
	H_1	2.2705	1.0585	0.9972	0.9383

2.3 Maximum Minimum Eigenvalue (MME) Detection

Maximum-minimum eigenvalue (MME) detection uses the ratio called test statistic $T = \lambda_{\max} / \lambda_{\min}$ and a preset threshold γ to detect the presence of PUs as follows:

$$\begin{cases} H_1 : T > \gamma \\ H_0 : T \le \gamma \end{cases}.$$ (2.7)

The concept of MME detection is to separate the subspaces of signal and noise via EVD. If the received vector is long enough, it can be guaranteed that the channel matrix **H** is of full column rank. In this case, the smallest eigenvalues of $\mathbf{R}_Y$ will contain only the information about noise but not the primary signals. This confirms the necessity of extending the received signal vector as described in Section 2.1.

Let $P_{fa} = P(T > \gamma \mid H_0)$ be the probability of false alarm and $P_d = P(T > \gamma \mid H_1)$ be the probability of detection. Since there is usually no information about the primary signal at the receiver side, we often analyze the threshold under H_0. Denote as l_{max} and l_{min} the normalized maximum and minimum eigenvalues of $R'_{vv}(N_s) = \left(N_s / \sigma_v^2\right) R_{vv}(N_s)$. It can be shown that when $N_s, ML \to \infty$, l_{max} and l_{min} converge to two constants as follows [19]:

$$
\begin{aligned}
l_{\min} &\to a = \left(N_s^{1/2} - \left(M \cdot L \right)^{1/2} \right)^2 \\
l_{\max} &\to b = \left(N_s^{1/2} + \left(M \cdot L \right)^{1/2} \right)^2 .
\end{aligned}
\tag{2.8}
$$

In [20], $L_{\max} = \left(l_{\max} - b \right) / \nu$ has been proved to converge to the cumulative distribution function (CDF) of Tracy-Widom of order 2 (TW$_2$) asymptotically. Here ν is the value depending on system parameters N_s and ML, that is

$$
\nu = \left(\left(N_s^{1/2} + \left(M \cdot L \right)^{1/2} \right)^2 \left(N_s^{-1/2} + \left(M \cdot L \right)^{-1/2} \right)^{1/3} \right).
\tag{2.9}
$$

By random matrix theory [7], under $N_s, ML \to \infty$, the asymptotic threshold is

$$
\gamma = \left(\frac{N_s^{1/2} + \left(ML \right)^{1/2}}{N_s^{1/2} - \left(ML \right)^{1/2}} \right)^2 \cdot \left(1 + \frac{\left(N_s^{1/2} + \left(ML \right)^{1/2} \right)^{-2/3}}{\left(N_s \cdot \left(ML \right) \right)^{1/6}} \right) F_{TW2}^{-1}(1 - P_{fa}),
\tag{2.10}
$$

where F_{TW2} denotes the CDF of TW$_2$. Since M, L, N_s are finite numbers; the threshold in (2.10) is only an approximate value. In practice, this threshold needs to be obtained by Monte Carlo simulations using the model described in Section 2.1.

The MME method performs a blind detection without knowledge of the channel, signal, and noise power. When noise uncertainty exists, the MME method can significantly outperform another blind detection method called energy detection.

The simulation of the detection performance of the MME method and energy detection is shown in Figure 2.3, in which each FAP is equipped with $M = 4$ antennas that senses $P = 2$ primary user in a specific spectral band with the observation window size $L = 8$. The channel is randomly generated in complex Gaussian distribution with $N=10$ taps, the number of samples is $N_s = 10000$ and false alarm rate is $P_{fa} = 0.1$, respectively. Figure 2.3 shows that a small noise uncertainty degrades the detection performance a lot. Finally, Table 2.3 gives the procedure of doing spectrum sensing with MME detection.
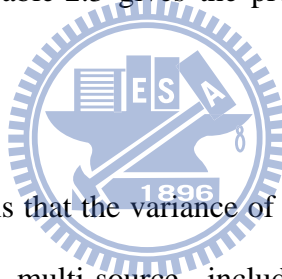
Note: noise uncertainty means that the variance of noise is not a constant [21]. In fact, noise is an aggregation of multi-source, including non-linearity of components, non-uniform or time-varying thermal noise, and interference due to transmissions by other users, etc. We define the noise uncertainty as

$$v_\alpha(n) \sim N(0,\sigma_\alpha^2) \quad \text{and} \quad \sigma_\alpha^2 \in \left[\frac{1}{\alpha}\sigma^2, \ \alpha\sigma^2\right], \tag{2.11}$$

where α denotes the noise uncertainty factor which is normally 1 to 2 dB.
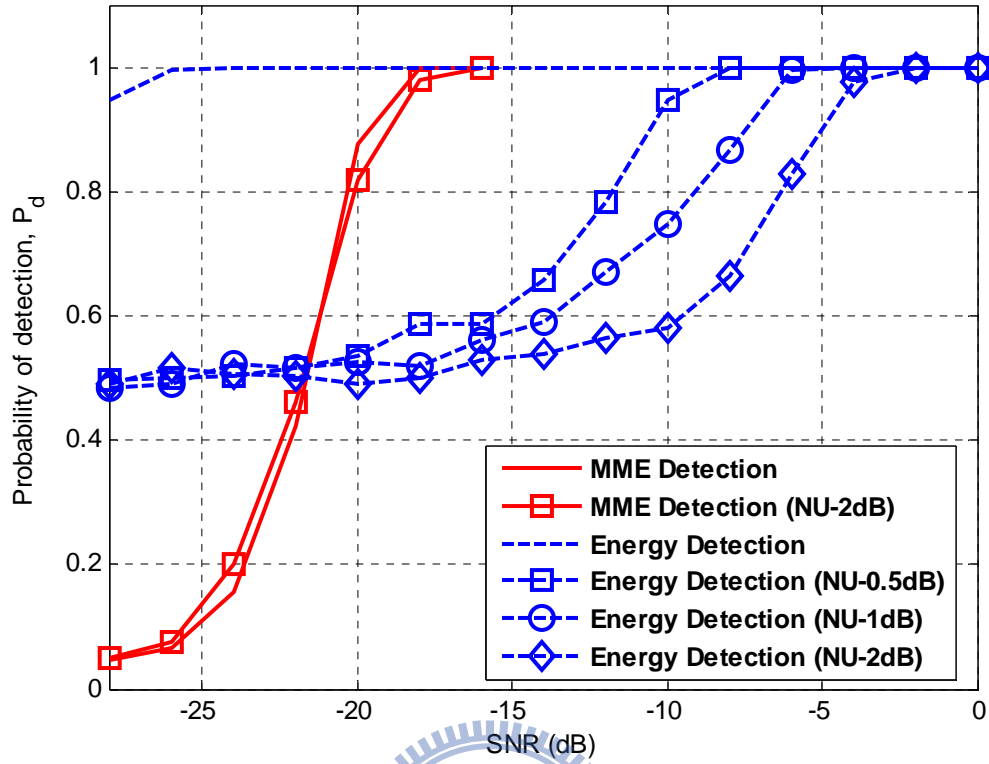
Figure 2.3: MME vs. energy detection ($M = 4$, $L = 8$, $P = 2$, $N = 10$, $N_s = 10^5$)

Table 2.3: Maximum-minimum eigenvalue (MME) detection

Step1	Compute the sampled covariance matrix of the received signal, that is $R_Y(N_s)$
Step2	Obtain the maximum and minimum eigenvalue of $R_Y(N_s)$,and compute the corresponding ratio $T = \lambda_{\max} / \lambda_{\min}$
Step3	Find the decision threshold γ corresponding to specific probability of false-alarm P_{fa}
Step4	Decision $\begin{cases} \mathcal{H}_1 : T > \gamma \\ \mathcal{H}_0 : T \leq \gamma \end{cases}$

2.4 Conventional MME-based Cooperative Spectrum Sensing

In conventional MME-based cooperative spectrum sensing [11], [19], [22], K base stations in the secondary system share their received signals $\{\mathbf{Y}_k\}$, whose size is $(M \cdot L) \times 1$, to build an aggregated observation vector $\mathbf{Y}_a$:

$$\begin{aligned}\mathbf{Y}_a(n) &= \begin{bmatrix}\mathbf{Y}_1(n) & \cdots & \mathbf{Y}_K(n)\end{bmatrix}^T \\ &= \begin{bmatrix}\mathbf{H}_1 & \cdots & \mathbf{H}_K\end{bmatrix}^T \cdot \mathbf{X}(n) + \mathbf{V}_a(n) \quad, n = 1, ..., N_s\end{aligned}, \tag{2.12}$$

FAPs share their entire received vector with others to build a longer received vector which is of size $(K \cdot M \cdot L) \times 1$. There are two motivations for us to build an aggregated observation vector $\mathbf{Y}_a$:

1. As we have discussed in Section 2.3, "the concept of MME detection is to separate the subspaces of signal and noise via EVD" and a longer received vector could separate the subspaces better and thus improve the detection performance.
2. Doing spectrum sensing jointly with other FAPs can avoid the hidden node problem or the bad channel condition, thus improving the sensing reliability.

The improvements of MME detector with different numbers of FAPs doing cooperative spectrum sensing are shown in Figure 2.4.
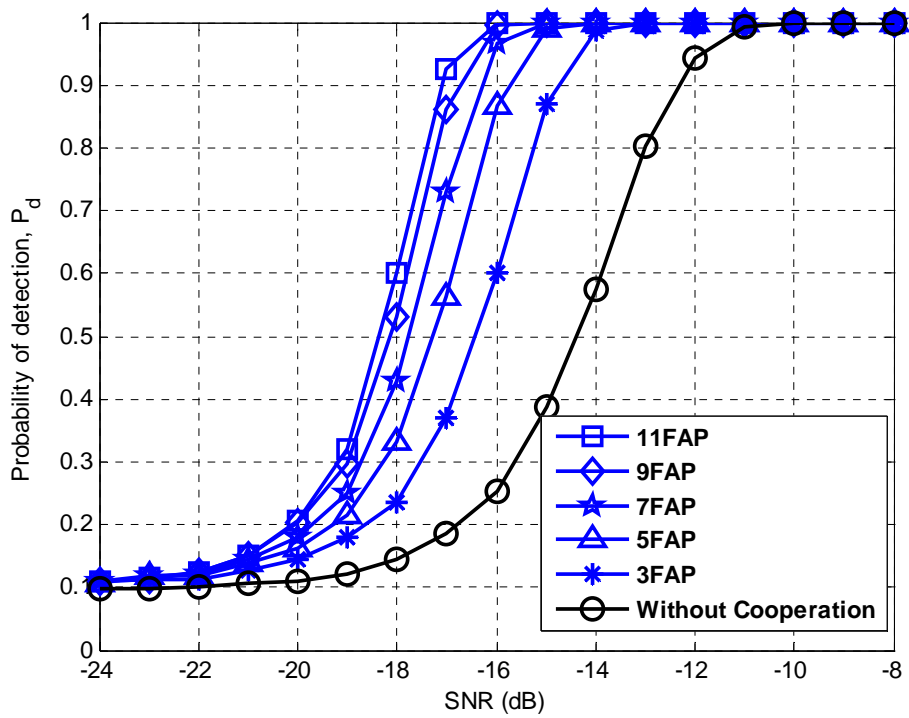
Figure 2.4: Probability of detection with different numbers of FAPs with the

MME-based cooperative spectrum sensing method

$(M = 4,\ L = 8,\ P = 1,\ N = 10,\ N_s = 1000)$

2.5 Summary

The basic ideas about the eigenvalues of covariance matrix and the MME-based cooperative spectrum sensing are introduced in this chapter. The most important concept of MME-based spectrum sensing is to use the EVD function to separate the information about the primary signal and noise power. The MME detection method is a kind of blind detection, thus it can be used for various signal detection without knowledge of the signal, channel, and noise power in heterogeneous networks. Another advantage of the MME method is that it's more reliable under noise uncertainty. Finally, based on MME detection, FAPs share their local sensing information to create a cooperative spectrum sensing algorithm which improves the probability of detection.
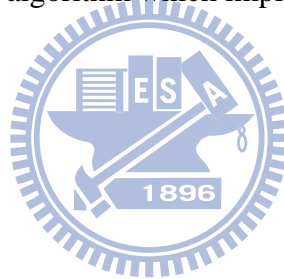
Chapter 3

The proposed MME-based Low Overhead Low Complexity Cooperative Method

In this chapter, we introduce a new cooperative method for MME-based spectrum sensing. In the proposed method, FAPs in the cluster exchange eigenvalues instead of the entire received signal vector as a metric for doing spectrum sensing. Moreover, we also introduce some reliability enhancement techniques to approach the detection performance of the conventional MME-based cooperative spectrum sensing method.

The conventional MME-based cooperative spectrum sensing method in Section 2.4 needs to exchange the full information of the received signal, which is of size $M \times L \times K \times N_s$, and compute the large covariance matrix with high complexity. In conventional CR networks, exchanging a huge amount of observations is made possible by sharing local information over a wired high speed backbone. However, the wired transmission is not applicable in femtocell-based heterogeneous networks in which the high speed backbones are usually not available. However, a stringent requirement of cooperative spectrum sensing is to lower the amount of exchanged sensory data and lower the computational complexity since the SU devices are usually low cost equipment. For these reason, we are motivated to develop a new cooperative spectrum sensing

scheme with low exchange overhead and low computational complexity, which make sharing information with other neighboring femtocells in the cluster via wireless broadcasting become possible.

The remainder of this chapter is organized as follows. In Section 3.1, the proposed low overhead low complexity cooperative method is presented. A further modification on the test statistic is described in Section 3.2. In Section 3.3, the comparison of the overhead and computational complexity between the proposed method and conventional method are discussed. Section 3.4 presents the numerical results of the proposed method, and Section 3.5 summarizes this chapter.

3.1 Eigenvalue-based Information Exchange Method

In this section, we propose a new cluster-based and distributed spectrum sensing scheme based on a modified MME method for CR networks. We define "Cluster-based" and "distributed" as follows:

● **Cluster-based**: FAPs falling in the same cluster as depicted in Figure 2.1 can exchange local information with their neighbors [23].

● **Distributed**: FAP acts as a sensing terminal as well as a fusion center; it could compute its own covariance matrix and eigenvalues beforehand and share with its neighbors. These eigenvalues are denoted as λ_j^k, $k = 1,...,K$. These K FAPs only exchange the eigenvalues instead of the entire received vectors. Thus the computational complexity and overhead can be reduced largely.

Optimization Problem Formulation

Our goal in this section is to maximize the detection probability through the weighted sum of the maximum and minimum eigenvalues, for which the optimization problem can be formulated as follows:

$$\arg\max_{\alpha_k, \beta_k} : \quad P_d^{opt} = P(T_{opt} > \gamma \mid H_1)$$

$$\text{subject to} : \begin{cases} T_{opt} = \dfrac{\sum_{k=1}^{K} \alpha_k \lambda_{\max}^k}{\sum_{k=1}^{K} \beta_k \lambda_{\min}^k} \\[2ex] P_{fa}^{opt} = P_{fa} \\ \sum_{k=1}^{K} \alpha_k = 1 \\ \sum_{k=1}^{K} \beta_k = 1 \\ \alpha_k, \beta_k \in [0,1] \end{cases} , \qquad (3.1)$$

where α_k and β_k are the optimization variables. In practice, this problem is difficult to solve. Therefore, we remove the second constraint in (3.1) to permit a slight difference in P_{fa} values for optimization.

On the other hand, consider another situation in which some FAP encounters a hidden node problem or a bad channel condition. Then its maximum eigenvalue is seriously affected by the channel condition and becomes relatively low. To avoid this problem, the maximum of the K maximum eigenvalues is used instead, that is $\lambda'_{\max} = \max\{\lambda_{\max}^k\}$. In contrast, the minimum eigenvalues represents the information about noise in the K FAPs, thus $\{\lambda_{\min}^k\}$ are averaged over FAPs to reduce the uncertainty. Consequently, the solution to (3.1) and the corresponding test statistic under the above approximation are given as below:

$$\alpha_k = \begin{cases} 1 , & k = \arg\max_k\{\lambda_{\max}^k\} \\ 0 , & \text{otherwise} \end{cases},$$

$$\beta_k = 1 / K, \tag{3.2}$$

$$\text{and } T' = \left(\frac{\lambda'_{\max}}{\lambda'_{\min}}\right) = \left(\frac{\max\{\lambda_{\max}^k\}}{\dfrac{1}{K}\displaystyle\sum_{k=1}^{K}\lambda_{\min}^k}\right).$$

Our modified MME-based cooperative sensing methods can provide the desired detection performance, which is shown in Figure 3.4 in Section 3.4.

3.2 Further Modification on Test Statistic

Both the conventional (Figure 2.4) and the proposed method (Figure 3.4) can enhance the performance of the MME detector with cooperation, and the comparison is shown in Figure 3.5 in Section 3.4. However, there are two major differences:

1. In high SNR regions, the detection probability P_d in the proposed method becomes worse than the conventional method.

2. In low SNR regions, the detection probability P_d is raised. The reason is that with the false-alarm constraint in (3.1) removed, P_d increases both in high and low SNR regions which causes P_d to saturate to a value higher than the false alarm rate set before (P_d should converge to P_{fa} when SNR goes to minus infinity). Thus, the problem of a raised false alarm rate needs to be solved.

In the following we will introduce two modifications on test statistic to overcome the above two problems.

Modification 1:

$$T'' = \left(\frac{\max\{\sum\limits_{d=1}^{D} \lambda_d^k\}}{\frac{1}{K} \sum\limits_{k=1}^{K} \sum\limits_{d=1}^{D} \lambda_{(ML-d+1)}^k} \right) = \left(\frac{\lambda''_{\max}}{\lambda''_{\min}} \right). \qquad (3.3)$$

To deal with the first problem, we collect not only the maximum and minimum eigenvalues but up to D maximum and minimum eigenvalues and then sum them up. This modification could effectively improve the detection performance since the maximum eigenvalue of the sampled covariance matrix $\lambda_1 \sim L_{\max}$ is a random variable and the distribution of λ_1 that has discussed in Section2.3. Furthermore, each eigenvalues, i.e. $\lambda_i \sim L_i$, $i = 1, 2, ..., ML$, are also random variables. Figure 3.1 is an example which shows the distribution of the largest and smallest four eigenvalues, i.e. $\lambda_1, ..., \lambda_4$, and $\lambda_{(ML-3)}, ..., \lambda_{ML}$, in the case with $\text{SNR} = -10\text{dB}$. To collect more eignvalues into the test statistic could effectively improve the detection performance by decreasing the uncertainty in the test statistic.

Modification 2:

$$\begin{aligned} T''' &= \alpha(\rho) \cdot T'' \\ &= \alpha(\rho) \cdot \left(\max\{\sum_{d=1}^{D} \lambda_d^k\} \ / \ \frac{1}{K} \sum_{k=1}^{K} \sum_{d=1}^{D} \lambda_{(ML-d+1)}^k \right), \end{aligned}$$

$$(3.4)$$

where

$$\alpha(\rho) = \begin{cases} 1 & , \rho > RI \\ \{\eta \mid \eta < 1\}, & \rho < RI \end{cases}.$$
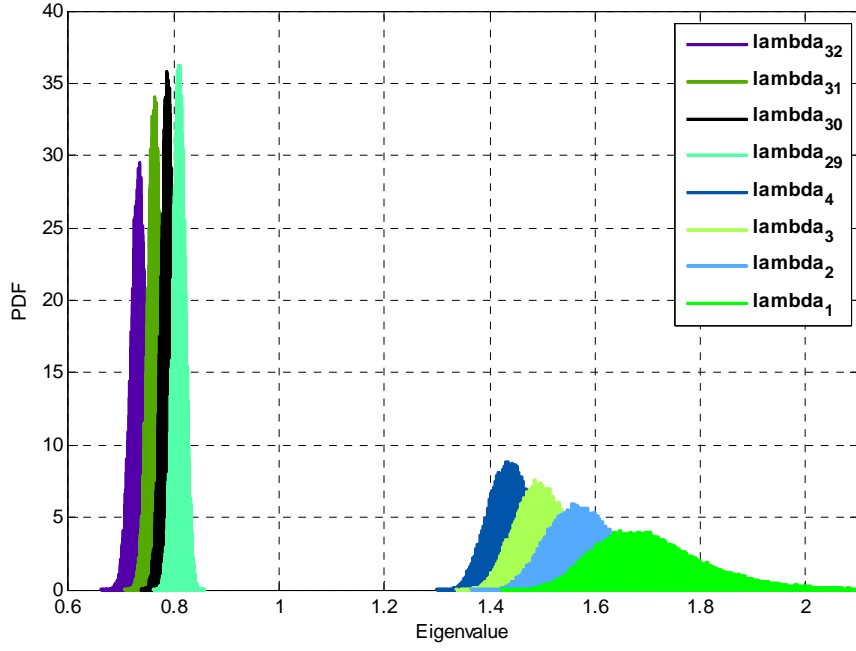
Figure 3.1: Distribution of the largest and smallest four eigenvalues

(M=4, L=8, P=1, N=10, N_s=1000, $\text{SNR} = -10\text{dB}$)

Another modification is to overcome the raised P_{fa} problem and we further modify the test statistic into (3.4), where $\alpha(\rho)$ is a suppression factor. In this modification, the SNR needs to be estimated first. If the estimated SNR ρ is below a threshold called "reliability indicator (RI)" of the primary signal, then multiply a constant $\{\eta \,|\, \eta < 1\}$ to suppress P_d. As we have mentioned above, when PUs are present, $\lambda_{\max}$ and $\lambda_{\min}$ are contributed by both signal and noise power, and the averaged ratio $E[\lambda_{\max} / \lambda_{\min}]$ should be related to SNR, as exemplified in Figure 3.2. This ratio can be pre-computed in a table and stored in the system.

One major criterion of setting of RI is that it should not affect the high SNR region performance especially for P_d>0.9, because this is the working region for FAPs and P_d often needs to be larger than 0.9 to avoid collision between signals from PUs and SUs.

Moreover, $E[\lambda_{\max} / \lambda_{\min}]$ becomes flat when SNR is low as shown in Figure 3.2. In this case, a small deviation in $E[\lambda_{\max} / \lambda_{\min}]$ corresponds to a large change in the estimated SNR and this would lead to that the true SNR is difficult to tell in the low SNR region. Therefore η should not be set too small or it may suppress the test statistic too much when the true SNR is larger than the RI.

Finally, the flowchart of the proposed eigenvalue-based information exchanging method is shown in Figure 3.3.
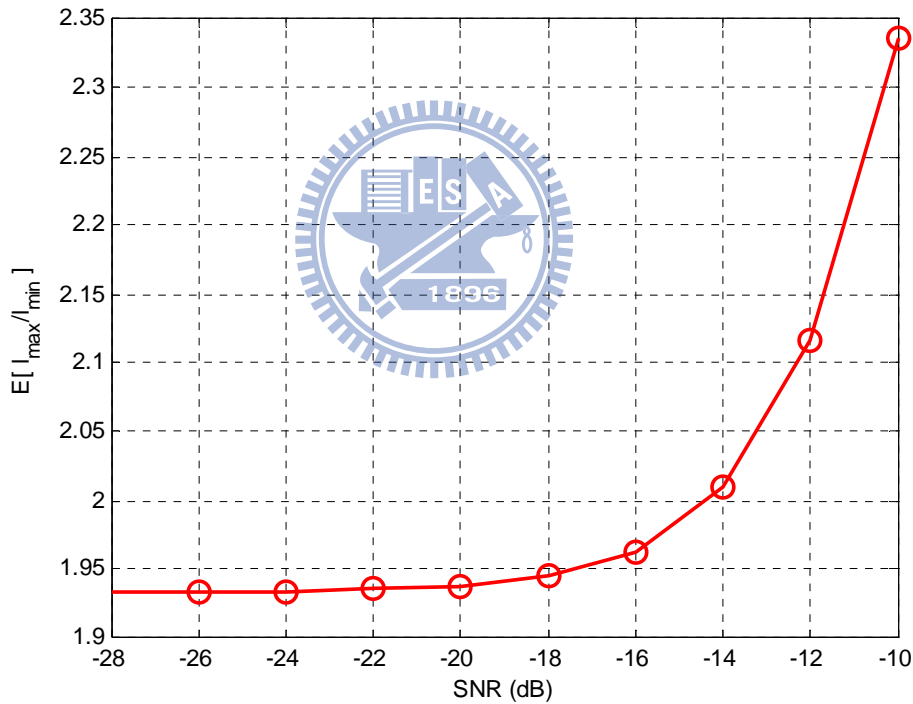
Figure 3.2: The relation between SNR and expected test statistic
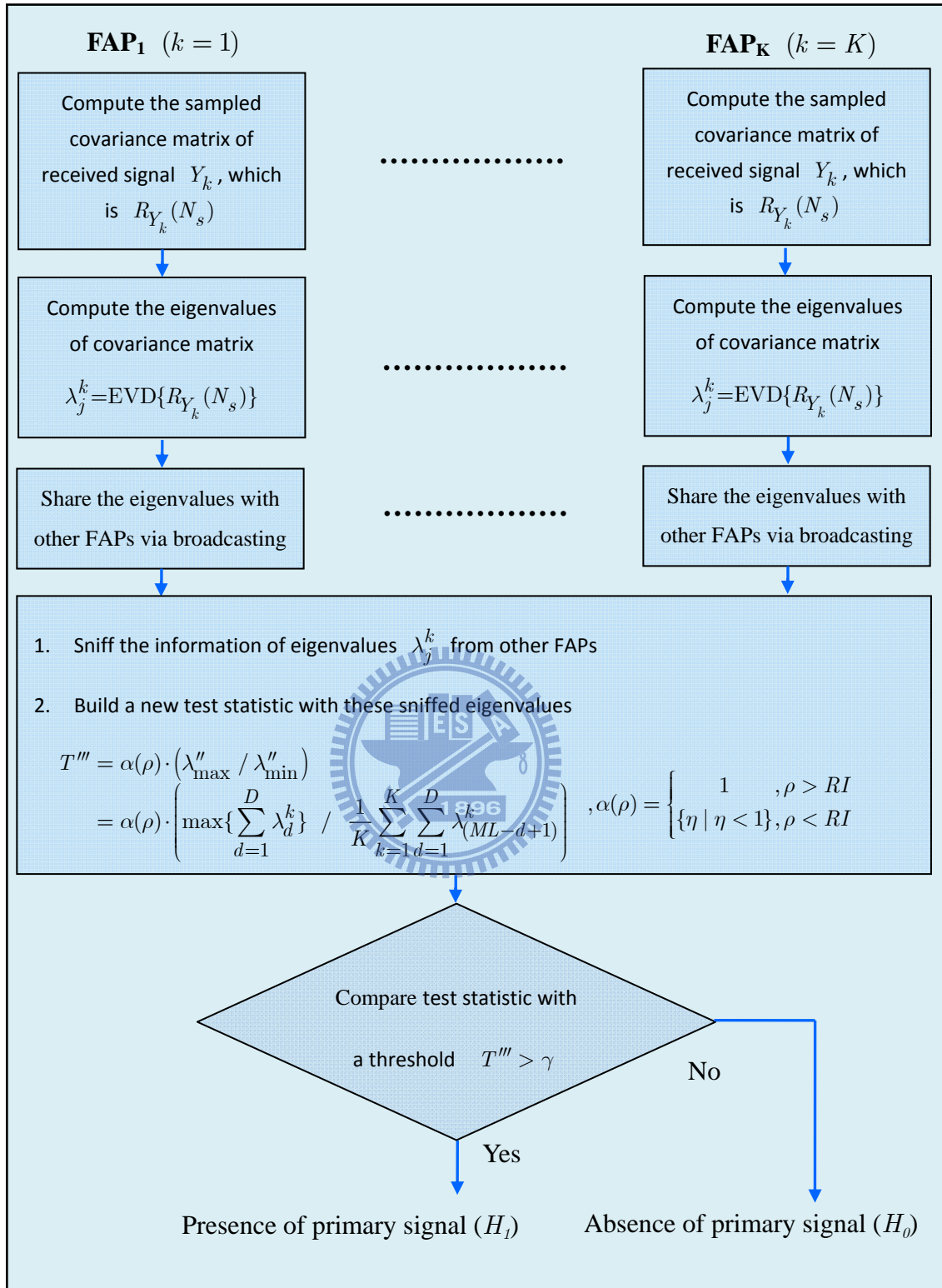
Figure 3.3: Flowchart of the eigenvalue-based information exchanging method

3.3 Complexity and Overhead Gain Analysis

1. **Complexity gain analysis:**

The major complexity of the eigenvalue-based algorithm comes from two parts:

(1) Computations of covariance matrix:

Since the covariance matrix of the received signal vector $\mathbf{Y}(n) = [y_1(n) \quad y_2(n) \quad \cdots \quad y_l(n)]^T$, $n = 1, 2, ..., N_s$ is Hermitian, we only need to compute the upper or lower triangular part of the covariance matrix. When the length of random vector is l, the number of multiplications and additions are given in (3.5).

$$
\begin{cases}
N_{mul} = N_s \cdot \left(\sum_{n=0}^{l-1} l - n \right) = N_s \left(\frac{l^2}{2} + \frac{l}{2} \right) \\
N_{add} = (N_s - 1)\left(\frac{l^2}{2} + \frac{l}{2} \right) \approx N_{mul}
\end{cases}
, \tag{3.5}
$$

where
$$
\begin{cases}
l = M \cdot L \cdot K \text{ , for conventional method} \\
l = M \cdot L \quad \text{ , for the proposed method}
\end{cases}.
$$

(2) Eigenvalue decomposition (EVD):

Complexity of EVD is the same to solve the characteristic function $\det\left[\mathbf{R}_y - \lambda \mathbf{I}_l\right]$, needs $O(l^3)$ multiplications and additions generally [24].

Finally, the total complexity (multiplications and additions) are therefore the composition of above two parts, which is

$$C_{cmp}(l) = N_s \left(\frac{l^2}{2} + \frac{l}{2} \right) + O(l^3),$$

(3.6)

where

$$\begin{cases} l = M \cdot L \cdot K & \text{, for conventional method} \\ l = M \cdot L & \text{, for the proposed method} \end{cases}.$$

Since N_s is usually larger than l ($N_s \gg l$), the first part will dominate, and the computational complexity of the conventional MME algorithm is generally K^2 times higher than the proposed modified algorithm.

2. Overhead gain analysis

The proposed algorithm simply needs to exchange some specific compressed information to other FAPs, i.e. $2D$ eigenvalues, instead of the whole observations. The total numbers of information exchanges via broadcasting in the proposed algorithm and with wired backbone in the conventional MME are given as follows:

$$\begin{cases} N_{bro} = M \cdot L \cdot N_s \cdot K & \text{, for conventional method} \\ N_{bro2} = 2 \cdot D \cdot K & \text{, for the proposed method} \end{cases}.$$

(3.7)

3.4 Computer Simulations

In this section, the simulation results of the proposed method mentioned in Section 3.2 and Section 3.3 are presented. In the simulations, each FAP is assumed to be equipped with $M = 4$ antennas that senses $P = 1$ primary user in a specific spectral band with the observation window size $L = 8$. The channel is randomly generated in complex Gaussian distribution with $N = 10$ taps, the number of samples is $N_s = 1000$, respectively. In IEEE 802.22, a wireless standard based on cognitive radios is [28], the requirement of false alarm rate in this standard is 0.1. Therefore, we choose $P_{fa} = 0.1$ in our work. All results in this section are obtained by Monte-Carlo simulations.

The detection probability of the proposed method with different numbers of FAPs doing cooperative spectrum sensing is shown in Figure 3.4 (without further modification). The proposed method outperforms that without cooperation by 1.5 dB and 3 dB, respectively, for the 3-FAP and 11-FAP scenarios when P_d=0.9. Figure 3.5 shows the comparison of detection probability between the conventional cooperative method (method 1) and the proposed cooperative method without modification (method 2). However, in the high SNR region above 18 dB, the detection probability of the proposed method increases more slowly with SNR than the conventional MME. This is because the conventional method uses a longer received vector which could separate the subspaces of signal and noise better and thus have better detection performance. On the other hand, in the low SNR region below 19 dB, the detection probability of the proposed method is raised especially for the 11-FAP case since we have removed the P_{fa} constraint mentioned in Section 3.2.1.
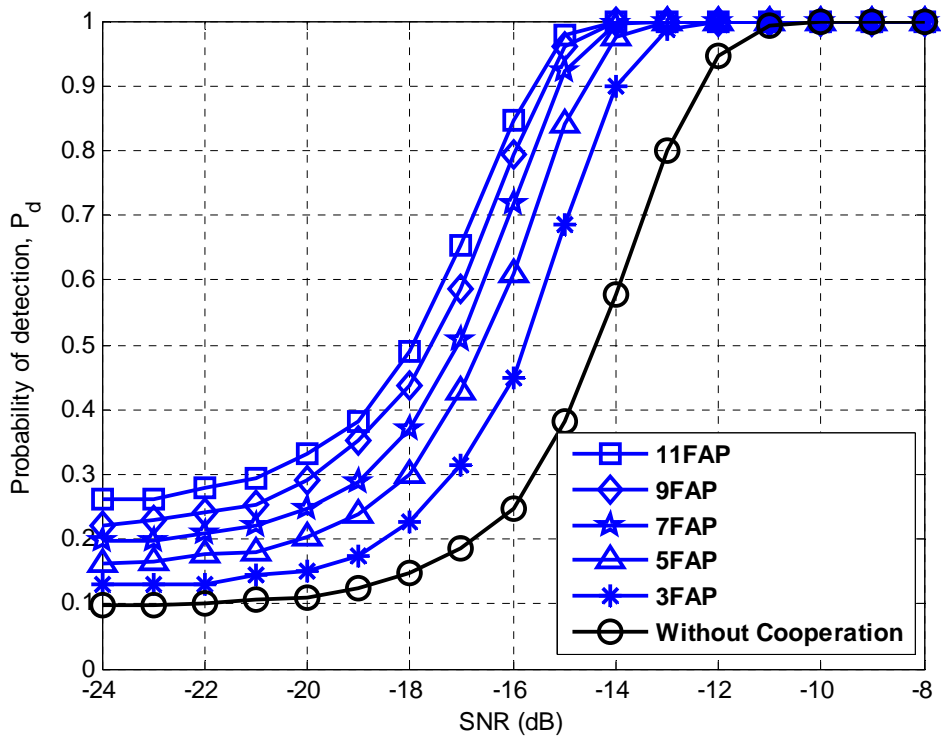
Figure 3.4: Detection probability of the proposed method with different numbers of

FAPs doing cooperative spectrum sensing
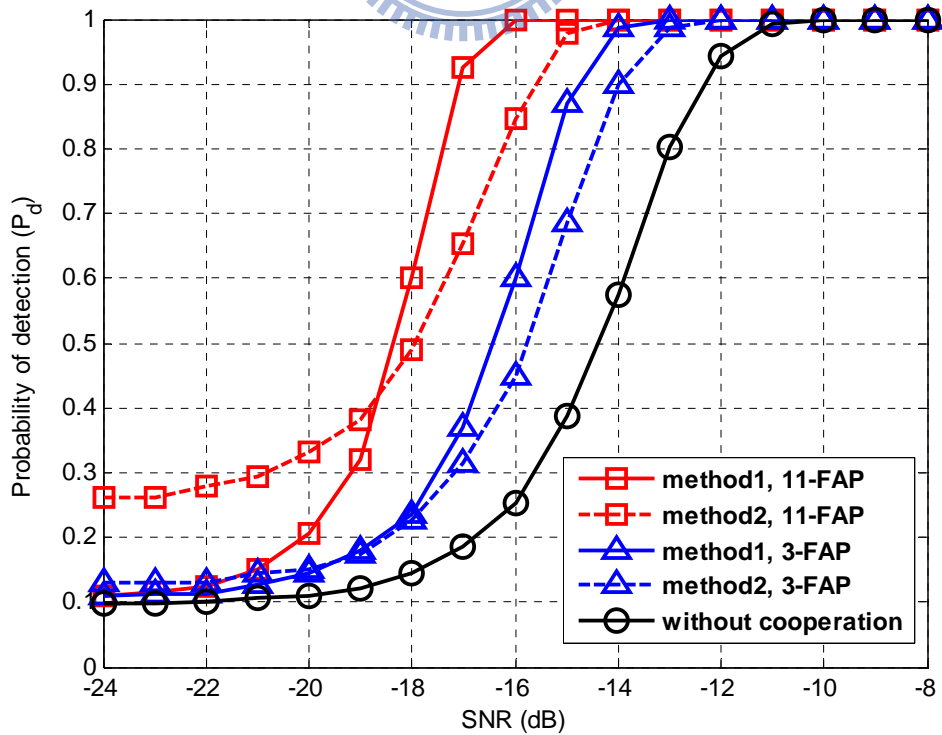
Figure 3.5: Probability of detection of method 1 and method 2

To approach the detection performance of the conventional method, two modifications are applied as described in Section 3.2.2. Figure 3.6 shows a significant enhancement with $D=8$, $RI_{3FAP}= -16$ dB and $RI_{11FAP}=-20$ dB. In the 3-FAP case, the conventional method and the modified method almost achieve the same detection probability. However, in the 11-FAP scenario in Figure 3.6, a raised P_d, is observed at low SNR. This is because that a low SNR cannot be accurately estimated and compared with RI. This could be fixed by choosing a small η as mentioned in Section 3.2.2. However, a too small η would cause the detection probability to drop too much in the large SNR region. Therefore a design trade-off is needed for choosing η which leads to some compromise between the detection performance in the low and high SNR regions. In other words, if the detection probability in low SNR is suppressed too much, the detection probability in high SNR would decrease.

Finally, the comparison of transmission overhead is shown in Figure 3.7, which confirms the advantage of the proposed algorithm as mentioned in Section 3.3. In contrast to the conventional MME-based method for CR networks, in which SUs share huge amount information; the proposed method reduces implementation complexity and incurs a much smaller delay time and overhead.
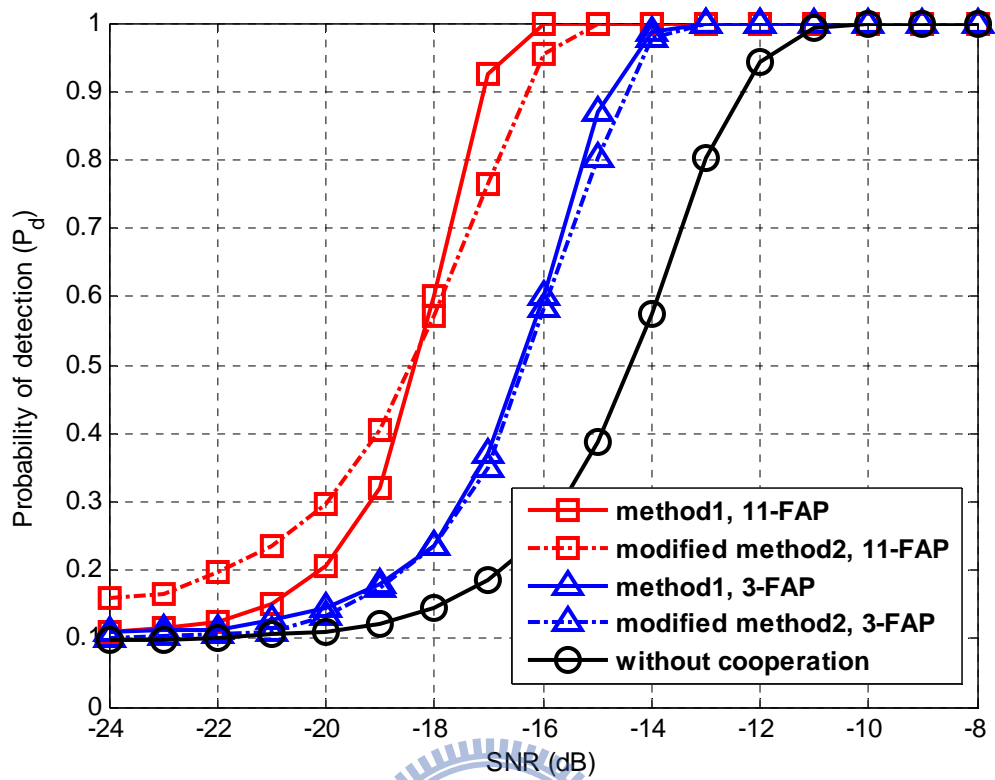
Figure 3.6: Probability of detection of method 1 and modified method 2
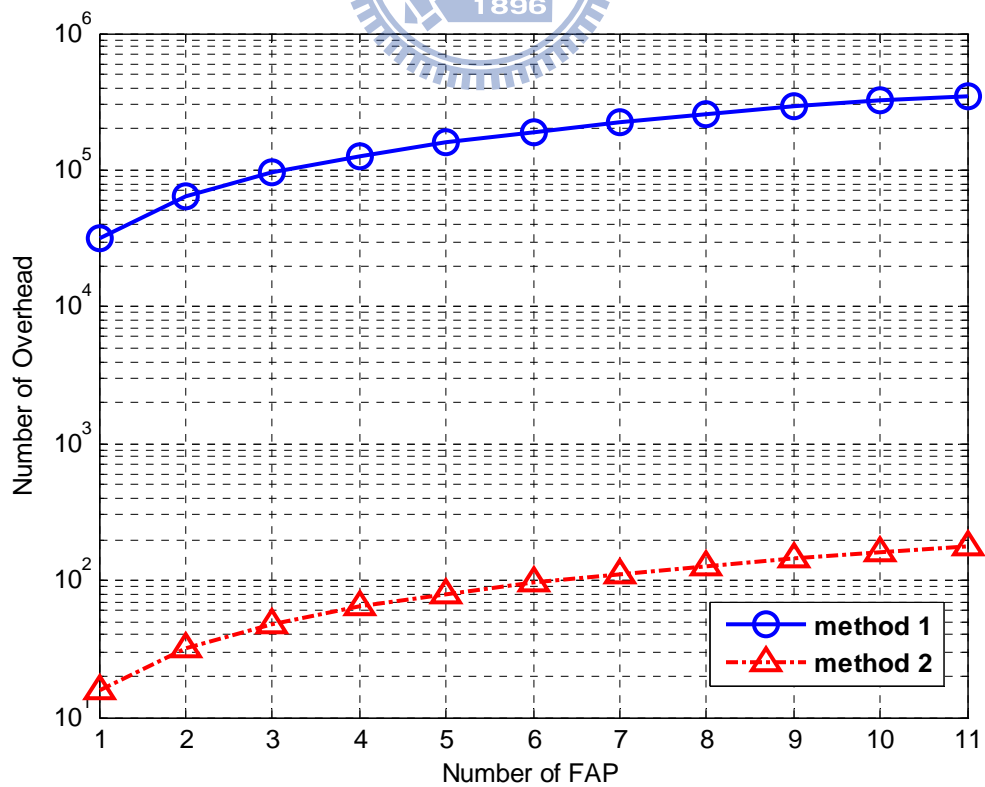
Figure 3.7: Transmission overhead in method 1 and method 2

3.5 Summary

In this chapter, we propose a decentralized cooperative spectrum sensing scheme with eigenvalue-based information exchange in cognitive femtocell networks. Two factors are introduced to ensure the detection reliability of the proposed scheme. The new scheme judiciously exploits wireless broadcasting information from neighboring femtocells. Compared with the conventional cooperative scheme, the proposed scheme exhibits similar detection performance while requiring a much lower overhead and complexity. Analysis of information exchange overhead and local computational complexity, as well as computer simulations confirms the effectiveness of the proposed cooperative spectrum sensing scheme in a femtocell network.
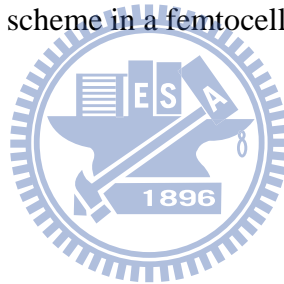
Chapter 4

Sensing-based Throughput Performance with Game-Theoretic Spectrum Allocation

Femtocell is a useful technique to increase the spectrum reuse factor. However, femtocells do not have the primary right to access the licensed RB. Therefore, the functionalities of spectrum sensing and resource allocation are needed. We have discussed the spectrum sensing technique in Chapter 2-3. In this chapter, we will further consider the spectrum allocation problem among femtocells with joint spectrum overlay and underlay strategy in the uplink OFDMA network. For this purpose, a useful algorithm called the regret-matching algorithm in game theory can provide an effective way to solve such a competition problem [17] [18]. Regret-matching algorithm is a kind of learning algorithm; the basic idea of regret-matching algorithm is to learn about the regret of its actions that had been taken at every time instant and aim at minimizing its regret value. In Section 4.1, we describe the spectrum sharing strategy between the PUs and SUs. In Section 4.2, the resource allocation problem is formulated as a non-cooperative game. The regret-matching algorithm can achieve the correlated equilibrium solution shown in Section 4.3. Section 4.4 shows the simulation results of this algorithm and Section 4.5 summarizes this chapter.

4.1 Joint Overlay and Underlay Spectrum Access Strategy

In order to increase the spectrum reuse factor, the spectrum sharing strategy between the PUs and SUs becomes an important issue. The most intuitive way called overlay spectrum access is to use the unoccupied portion of spectrum (RB). Hence, we need the spectrum sensing technique to differentiate between the occupied and unoccupied RBs. Practically, spectrum sensing cannot detect the existence of PUs perfectly. Moreover, there still has a problem of insufficient amount of available RBs. Thus, another method called underlay spectrum access is introduced. With the underlay spectrum access strategy, the SUs reuse the RBs that have been originally used by the PUs on the promise of not causing unacceptable interference to the PUs [25].

We consider the scenario depicted in Figure 2.1, in which a macrocell (PU) system coexists with a number of femtocell systems (SU) in an uplink OFDMA network. The sensing technique has mentioned in Chapter 3 and the effect of imperfect spectrum sensing can be described with two parameters, which are

$$\begin{cases} P_d = \text{pr}\{\text{consider busy} \mid \text{channel is busy}\} \\ P_{fa} = \text{pr}\{\text{consider busy} \mid \text{channel is idle}\} \end{cases}. \tag{4.1}$$

The effects of these two parameters are shown in Figure 4.1 (The parameters shown in Figure 4.1 are given in Table 4.1). To easily represent the effect of the above two parameters, we firstly rearrange the order of RBs (every MUEs are originally occupied by a RB). The effect of P_{fa} is to waste the opportunity for transmission and therefore reduces the frequency reuse factor. As we have discussed in Chapter 3, the detection probability P_d depends on the SNR at receiver side. Since the geographic parameters

of every MUEs are unique, P_d in every RBs are also unique. When P_d goes down with a low SNR, i.e. MUE is far from FAP, we cannot detect the existence of MUEs correctly. In practice, we can reuse those used RBs because the cross-tier interference between the FUEs and MUEs is low.
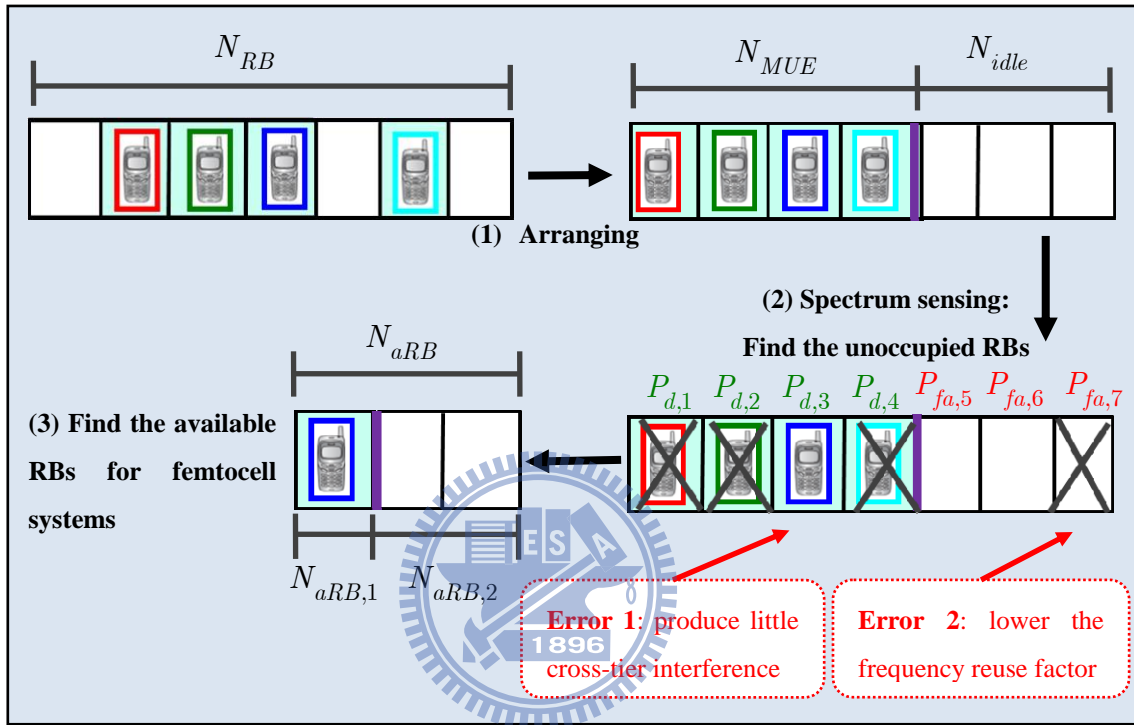
Figure 4.1: Illustration of the effect of imperfect spectrum sensing

Table 4.1: The parameters in Figure 4.1

N_{RB}	Total number of RBs
N_{MUE}	Number of MUEs
N_{idle}	Number of idle RBs which are unoccupied by MUEs ($N_{idle} = N_{RB} - N_{MUE}$)
$N_{aRB,1}$	Number of avaliable RBs with cross-tier interference
$N_{aRB,2}$	Number of avaliable RBs without cross-tier interference
N_{aRB}	Total number of avaliable RBs ($N_{aRB} = N_{aRB,1} + N_{aRB,2}$)

4.2 Game Formulation for Spectrum Allocation Problem

After the spectrum sensing phase, the problem is to allocate those RBs among femtocell users. To reach the goal, we firstly formulate our problem into a game form and solve it with regret-matching algorithm in the next section. To describe a game, the following four elements are included [13]:

- **Game**: We formulate the spectrum (RB) allocation problem among femtocell users in the same cluster in the uplink LTE system as a non-cooperative game. In game theory, the non-cooperative game means that all players make their own decisions independently. The non-cooperative game has a distributed nature as each FAP does not require the information of others. Consequently, the increasing of number of FUEs does also not raise the system computational complexity.

- **Player**: The K FUEs coexisting in the same cluster are modeled as players competing to acquire the available RBs.

- **Actions**: Which RB chosen by the FAP is defined as an action. We use a vector $\mathbf{a}_k^t$ to denote the action taken by the kth FAP at time instant $t = 1,\ldots,\mathrm{T}$, which is

$$\begin{cases} \mathbf{a}_k^t = \left[a_k^t(1),\ldots, a_k^t(N_{aRB}) \right] \in \mathcal{A}_k \\ \sum_{f=1}^{N_{aRB}} a_k^t(f) = 1, \end{cases}, \qquad (4.2)$$

where $a_k^t(f) \in \{0,1\}$ represents the fth RB is used for the kth FUE or not, where 0 represents *not use* and 1 represents *use*. $\mathcal{A}_k$ denotes the action space (a set of

actions) of the kth FAP, and we use $\left|\mathcal{A}_k\right|$ to denote the size of action space of the kth FAP, i.e. the number of different actions can be taken by FAP. N_{aRB} represents the number of available RBs occupied by femtocells and $\sum_{f=1}^{N_{aRB}} a_k^t(f) = 1$ denotes the maximum number of available RBs can be chosen by FAPs is one. Moreover, a matrix $\mathbf{a}^t$ is used to denote the joint action of K FAPs. The detail of $\mathbf{a}^t$ is shown below:

$$\mathbf{a}^t = \left[\left(\mathbf{a}_1^t\right)^{\mathrm{T}}, \ldots, \left(\mathbf{a}_K^t\right)^{\mathrm{T}}\right]^{\mathrm{T}} \in \mathcal{A}, \tag{4.3}$$

where $\mathcal{A} \triangleq \prod_{k \in K} \mathcal{A}_k$ denotes the joint actions space of K FAPs (a set of joint actions) and it is of size $\left|\mathcal{A}\right| = \prod_{k=1}^{K} \left|\mathcal{A}_k\right|$. As we mentioned before, all players make their own decisions and do their actions independently in the non-cooperative game.

- **Utility function**: Let U_k^t denotes the local utility function of FAP k at time instant t shown in (4.3). Here "local" means that each FAP in the cluster only has the information about its own action $\mathbf{a}_k^t$, but not have any information about other FAPs' actions, which are $\{\mathbf{a}_i^t, \ i = 1, \ldots, K, \ i \neq k\}$. Thus, each FAP has its own utility. The detail of local utility is shown as follows:

$$U_k^t(\mathbf{a}^t) = \sum_{f=1}^{N_{aRB}} \log_2 \det\left[\mathbf{I}_M + \frac{a_k^t(f)}{\left[I_{ff,k}^{t}(\mathbf{a}^t) + I_{mf,k}^{t}(\mathbf{a}^t) + \sigma_k^2(f)\right]} \mathbf{H}_k(f)\mathbf{H}_k^{\mathrm{H}}(f)\right],$$

$$I_{ff,k}^{t}(\mathbf{a}^t) = \sum_{i=1}^{K} w_{ff_{k,i}}(f)\cdot a_i^t(f),$$

$$I_{mf,k}^{t}(\mathbf{a}^t) = \sum_{i=1}^{N_{MUE}} w_{mf_{k,i}}(f)\cdot a_i^t(f), \qquad k = 1,2,...K,$$

$$\sigma_k^2(f) = (N_0 - 30) + 10\log_{10}(W) + N_{fig},$$

(4.4)

where $\mathbf{H}_k^t(f)$ is the combination of path-loss and fast fading channel gain between the

kth FAP and its associated FUE. M is the number of FAP antennas. Let $\sigma_k^2(f)$ be the

variance of the AWGN channel at the kth FAP. We denote $I_{ff,k}^{t}$ and $I_{mf,k}^{t}$ as the

femto-to-femto interference (co-tier interference) and the macro-to-femto interference

(cross-tier interference) at time instant t, respectively. The co-tier interference matrix

$w_{ff_{k,i}}(f)$, which is of size $K \times K$, describes the co-tier interference between the kth

and the ith FAP. Assuming channel reciprocity, $w_{ff_{k,i}}(f)$ is a symmetric matrix and

the diagonal elements equal zeros. The cross-tier interference matrix $w_{mf_{k,i}}(f)$, which

is of size $K \times N_{MUE}$, describes the cross-tier interference between the kth FUE and

the ith MUE. Let W be the bandwidth of each RB and N_0, N_{fig} denote the thermal

noise density (dBm/Hz) and noise figure respectively [27].

4.3 Correlated Equilibrium Solutions with Regret-Matching algorithm

The global resource allocation optimization problem is to maximize the sum of each local utility function, which can be represented as follows:

$$\arg\max_{\mathcal{A}} \sum_k U_k^t\left(\mathcal{A}\right).$$
(4.5)

If the action spaces of every FAPs are the same, the size of joint action space becomes $\left|\mathcal{A}\right| = \left|\mathcal{A}_k\right|^K$. An easy way to find the global optimum solution is the exhaustive search method. However, the search space is up to $\left|\mathcal{A}_k\right|^K$ which result in a high computational complexity. Another problem is that the global optimum solution depends on the private information of every FAPs. Since femtocell is an undefined and user-plug-in system, such kind of assumption is not practical. For this reason, to maximize the global resource, an allocation scheme using a decentralized approach is needed.

To reach the global optimum solution with the decentralized approach, we borrow an idea from regret-matching algorithm in game theory [13] [17]; therefore, the spectrum access strategy becomes an adaptive extension of the regret-matching algorithm. The basic idea of regret-matching algorithm is to learn the regret of its own actions that had been taken at every time instant and aim at minimizing its regret value. The definitions of "regret" and "regret-matching algorithm" are shown below [18]:

- **Regret**: increase in utility such a change had always been made in the past.

- **Regret-matching algorithm**: switch to a different action in next time instant with a probability that is proportional to the regret of actions.

If all players in the game follow the regret-matching algorithm to switch their action, then the distribution of joint action space converges to a set of correlated equilibrium [17]. A simple explanation of equilibrium is that each player has chosen a prior action and no any player can increase its own local utility by changing its own action while the actions of other players are not changed. Under this condition, the set of actions are called equilibrium. Correlated equilibrium is a more general form of equilibrium, which is a probability distribution over the set of action space, and the definition of correlated equilibrium is shown below [13]:

$$\sum_{\mathbf{a}_{-k}^{t} \in \mathcal{A}_{-k}} \pi_{CE}\left(\mathbf{a}_{k}^{t}, \mathbf{a}_{-k}^{t}\right) \cdot U_{k}(\mathbf{a}_{k}^{t}) \geq \sum_{\mathbf{a}_{-k}^{t} \in \mathcal{A}_{-k}} \pi_{CE}\left(\widehat{\mathbf{a}}_{k}^{t}, \mathbf{a}_{-k}^{t}\right) \cdot U_{k}(\widehat{\mathbf{a}}_{k}^{t}), \ k = 1, 2, ..., K.$$

(4.6)

where $\left(\mathbf{a}_{k}^{t}, \mathbf{a}_{-k}^{t}\right) = \mathbf{a}^{t}$ is defined as the instantaneous action of the kth player at time instant t, i.e. ($\mathbf{a}_{k}^{t}$), and action of all players except the kth player, i.e. ($\mathbf{a}_{-k}^{t}$). $\pi_{CE}\left(\mathbf{a}_{k}^{t}, \mathbf{a}_{-k}^{t}\right)$ is the probability distribution of correlated equilibrium on joint action space $\mathcal{A}$.

We use matrix $\mathbf{G}_{k}(\mathbf{a}^{t})$ to denote the instantaneous regret values of the kth FAP at time t and the size of $\mathbf{G}_{k}(\mathbf{a}^{t})$ is $\left|\mathcal{A}_{k}\right| \times \left|\mathcal{A}_{k}\right|$. S_{j} and S_{i} denote the current and next action playing by FAPs, respectively ($S_{j}, S_{i} \in \mathcal{A}_{k}$). The element of the instantaneous regret matrix is shown below:

$$G_{k}^{(j,i)}(\mathbf{a}^{t}) = 1_{(\mathbf{a}_{k}^{t} = S_{j})} \times \left[U_{k}(S_{i}, \mathbf{a}_{-k}^{t}) - U_{k}(S_{j}, \mathbf{a}_{-k}^{t})\right], \ k = 1, 2, ..., K, \quad (4.7)$$

where $1_{(.)}$ is an indicator function. We use the matrix $\boldsymbol{\theta}_{k}^{t}$ to denote the overall regret value of the kth FAP at time t, which is also of size $\left|\mathcal{A}_{k}\right| \times \left|\mathcal{A}_{k}\right|$. The detail of $\boldsymbol{\theta}_{k}^{t}$ is
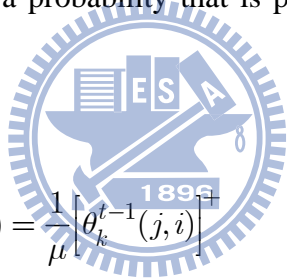
shown as follows:

$$\boldsymbol{\theta}_k^t = \boldsymbol{\theta}_k^{t-1} + \varepsilon^t \cdot \left(\mathbf{G}_k(\mathbf{a}^t) - \boldsymbol{\theta}_k^{t-1} \right)$$
$$= (1 - \varepsilon^t) \cdot \boldsymbol{\theta}_k^{t-1} + \varepsilon^t \cdot \mathbf{G}_k(\mathbf{a}^t), \ k = 1, 2, ..., K, \quad (4.8)$$

where $\varepsilon^t = 1 / t$ is a decreasing step size, which is used to accumulate the instantaneous regret value into the overall regret value. The entries of the overall regret matrix $\boldsymbol{\theta}_k^t$ denote the averaged regret value of user k until time t, which is denoted as

$$\theta_k^t(j, i) = \frac{1}{t} \sum_{\tau < t, \mathbf{a}_k^t = S_j} \left(U_k(S_i, \mathbf{a}_{-k}^\tau) - U_k(S_j, \mathbf{a}_k^\tau) \right), \ k = 1, 2, ..., K. \quad (4.9)$$

When the overall regret value has been computed, the action in next period will switch to action S_i from S_j with a probability that is proportional to the regret value, the detail is shown as follows:

$$\begin{cases} \mathrm{P}(\mathbf{a}_k^t = S_i \mid \mathbf{a}_k^{t-1} = S_j, \theta_k^{t-1}) = \frac{1}{\mu} \left[\theta_k^{t-1}(j, i) \right]^+ & , \text{ switch to } S_i \text{ from } S_j \\ \\ \mathrm{P}(\mathbf{a}_k^t = S_j \mid \mathbf{a}_k^{t-1} = S_j, \theta_k^{t-1}) = 1 - \frac{1}{\mu} \sum_{i \neq j} \left[\theta_k^{t-1}(j, i) \right]^+ & , \text{ stay in } S_j \end{cases} , \quad (4.10)$$

where $\mu > \sum_{i \neq j} \left[\theta_k^{t-1}(j, i) \right]^+$ is a constant to ensure that the probability is non-negative.

The structures of two kinds of regret matrix are shown in Figure 4.2 and Figure 4.3. Finally, Figure 4.4 gives the procedure of RB allocation with the regret-matching algorithm and compares the regret-matching algorithm with the learning algorithm.
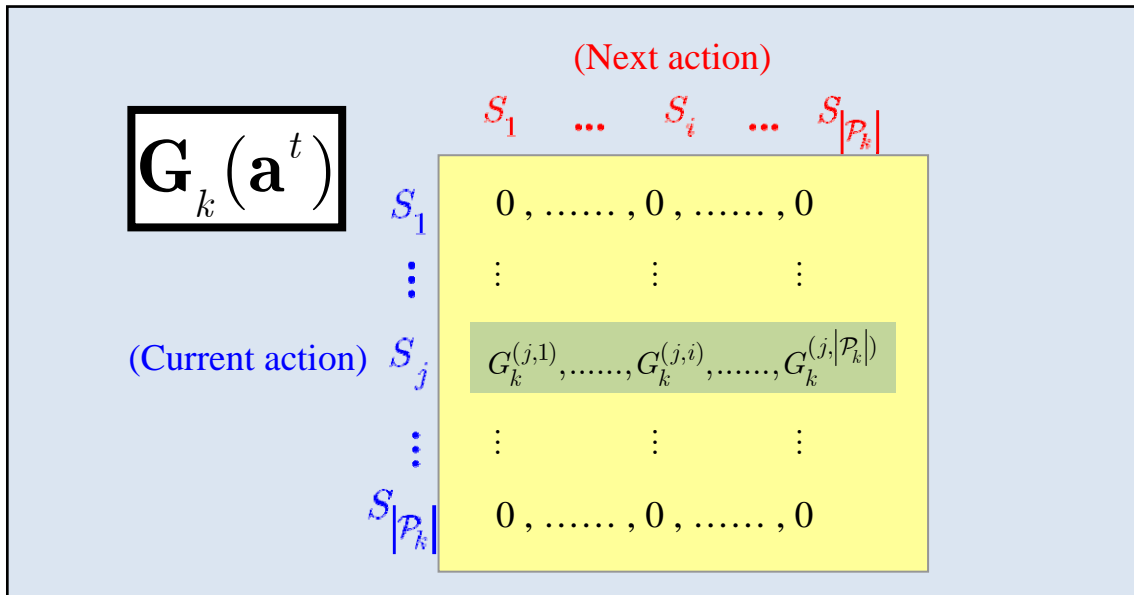
Figure 4.2: The structure of the instantaneous regret matrix
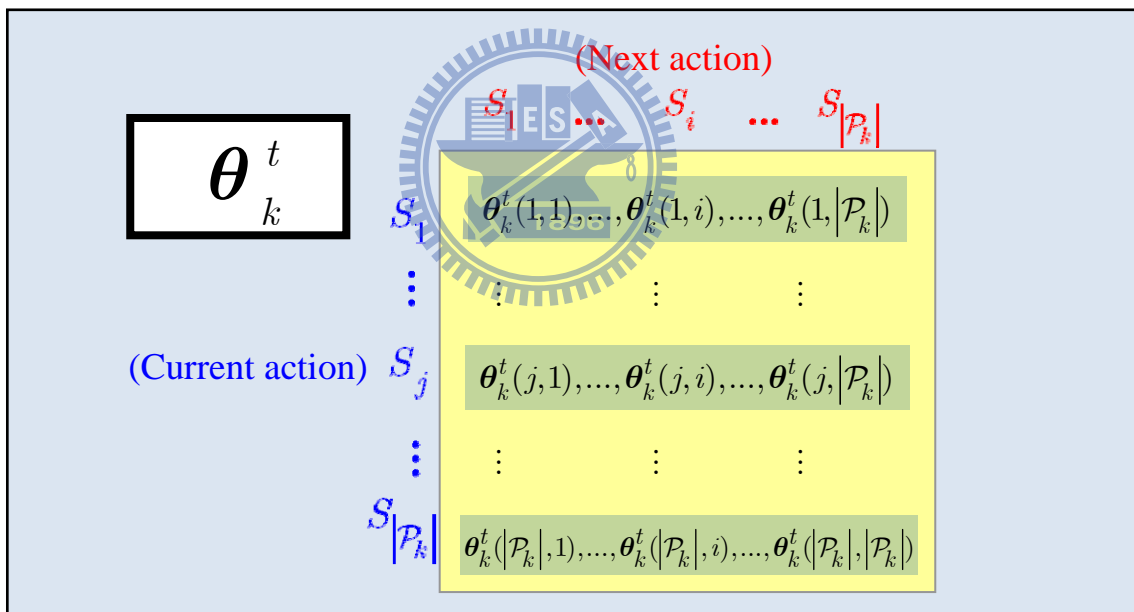
Figure 4.3: The structure of the overall regret matrix

Learning algorithm	Regret-matching algorithm

- **Start**

  ➤ Prior beliefs

- **Start** $(t = 0)$

  ➤ Find the available RBs via cooperative sensing

  ➤ Initialize $\mathbf{a}_k^0$ and $\theta_k^0 = \mathbf{H}_k(\mathbf{a}^0), \ \forall k \in K$

- **Step**

  ➤ Observe

- **Step** $(t = 1, 2, 3\ldots) \ \forall k \in K$

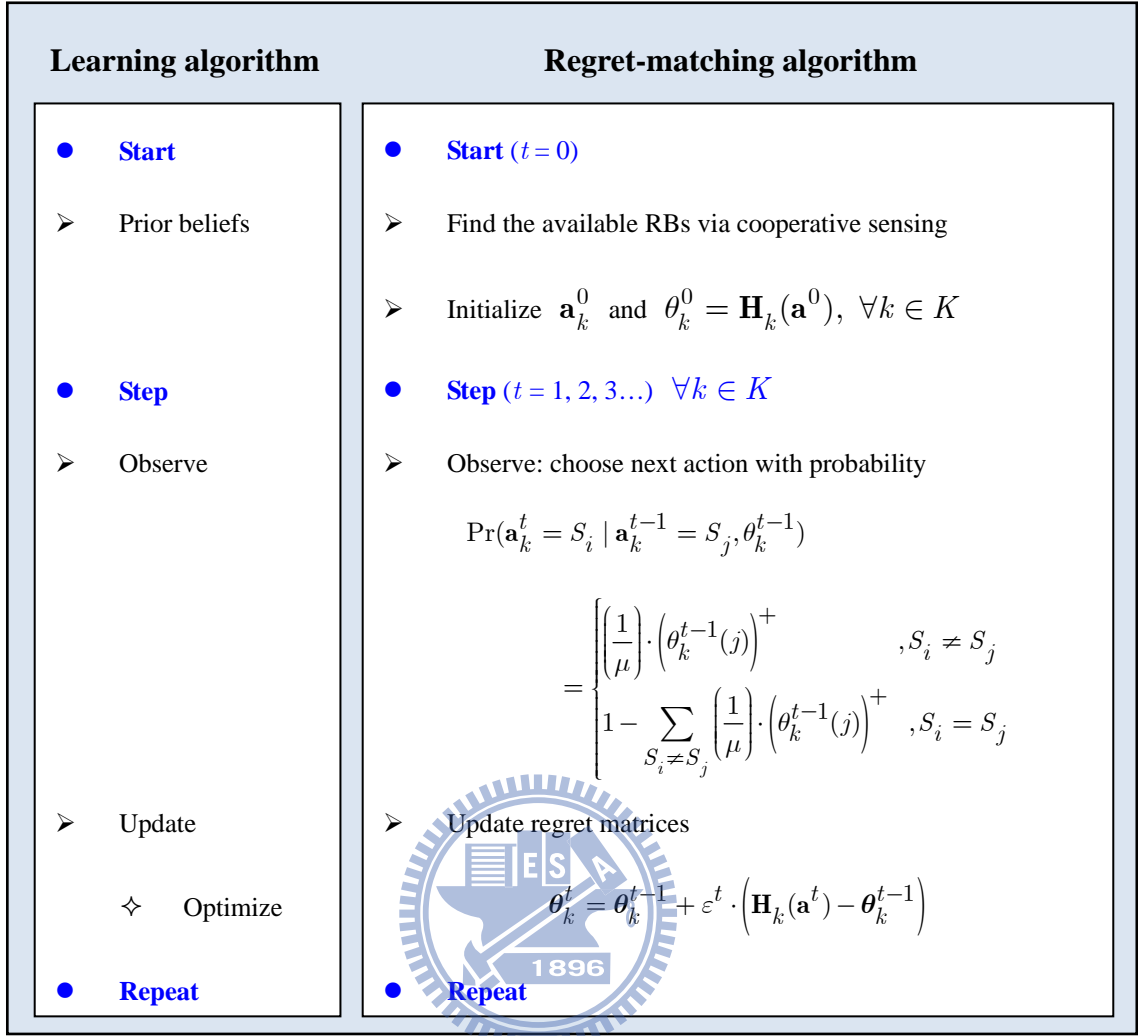 ➤ Observe: choose next action with probability

  $$\Pr(\mathbf{a}_k^t = S_i \mid \mathbf{a}_k^{t-1} = S_j, \theta_k^{t-1})$$

  $$= \begin{cases} \left(\dfrac{1}{\mu}\right) \cdot \left(\theta_k^{t-1}(j)\right)^+ & , S_i \neq S_j \\[2mm] 1 - \displaystyle\sum_{S_i \neq S_j} \left(\dfrac{1}{\mu}\right) \cdot \left(\theta_k^{t-1}(j)\right)^+ & , S_i = S_j \end{cases}$$

  ➤ Update

  ◇ Optimize

  ➤ Update regret matrices

  $$\theta_k^t = \theta_k^{t-1} + \varepsilon^t \cdot \left(\mathbf{H}_k(\mathbf{a}^t) - \theta_k^{t-1}\right)$$

- **Repeat**

- **Repeat**

Figure 4.4: The procedure of RB allocation with regret-matching algorithm

4.4 Computer Simulations

In this section, the simulation results of the proposed sensing-based throughput performance with game-theoretic resource allocation are presented. In the simulation, the environment parameters are shown in Table 4.2. The location of FAP and FUE are randomly distributed and underlaid with the macrocell. Moreover, each FAP serves one FUE within the femtocell coverage, which is shown in Figure 4.5.

Table 4.2: The environment parameters

| Parameter	Value
Macrocell coverage	Radius 500 m
Femtoocell coverage	Radius 100 m
FUE transmit power	26 dBm
MUE transmit power	26 dBm
Path loss model [26]	3GPP TR36.814 v9
Fading channel	Rayleigh
Average times of regret-matching algorithm	1000
Resource block bandwidth	180k Hz
Thermal noise PSD	-174 dBm/Hz
Noise figure	9 dB
Number of antennas of FAP	4
Number of antennas of FUE and MUE	1
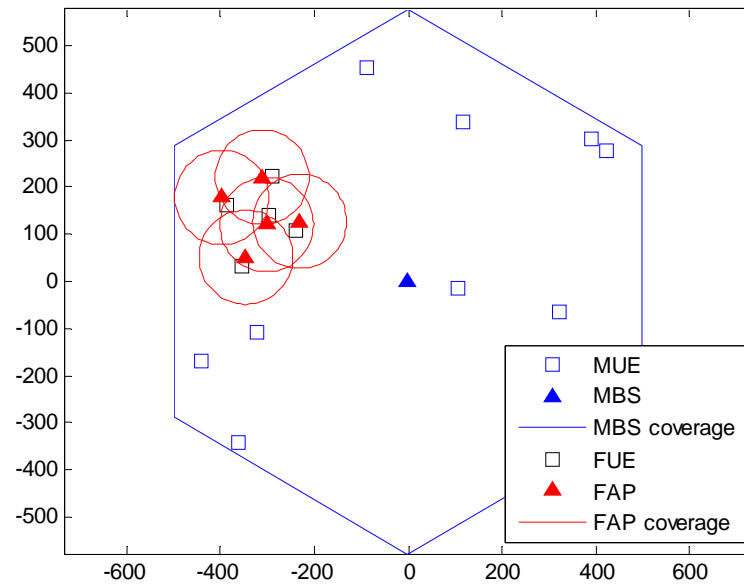
**Figure 4.5**: The distribution of MBS, MUE, FAP, and FUE, respectively

In Figure 4.6-4.8, we plot the average utility with a pure overlay spectrum access strategy. Pure overlay also means that each FAP has perfect sensing performance, i.e. $P_d = 1$ and $P_{fa} = 0$. The legends in Figure 4.6-4.8, i.e. {K FAP, N_{MUE} MUE, N_{RB} RB}, represents the situation that there are N_{MUE} RBs firstly occupied by MUEs, and FAPs can use the rest of $N_{aRB} = N_{idle} = (N_{RB} - N_{MUE})$ idle RBs.

In Figure 4.6, the average utilities with different number of FAPs are compared. Because of the distributed nature of regret-matching algorithm, the computational complexity of each local device (FAP) is not increased while the number of FAPs (players) is increased. In contrast, the convergence time (iteration index) is increased slightly when the number of FAPs is increased. The benchmark case, i.e. the exhaustive search method, is shown in Figure 4.7 and the distributed approach with regret-matching algorithm mentioned in Section 4.2 can approach the global optimal performance in about 60-80 iterations. This is because the regret value becomes smaller when the iterations are increased. A smaller regret value also means the co-tier interference between FAPs become smaller, thus we can find the best policy to allocate RBs with the smallest co-tier interference.
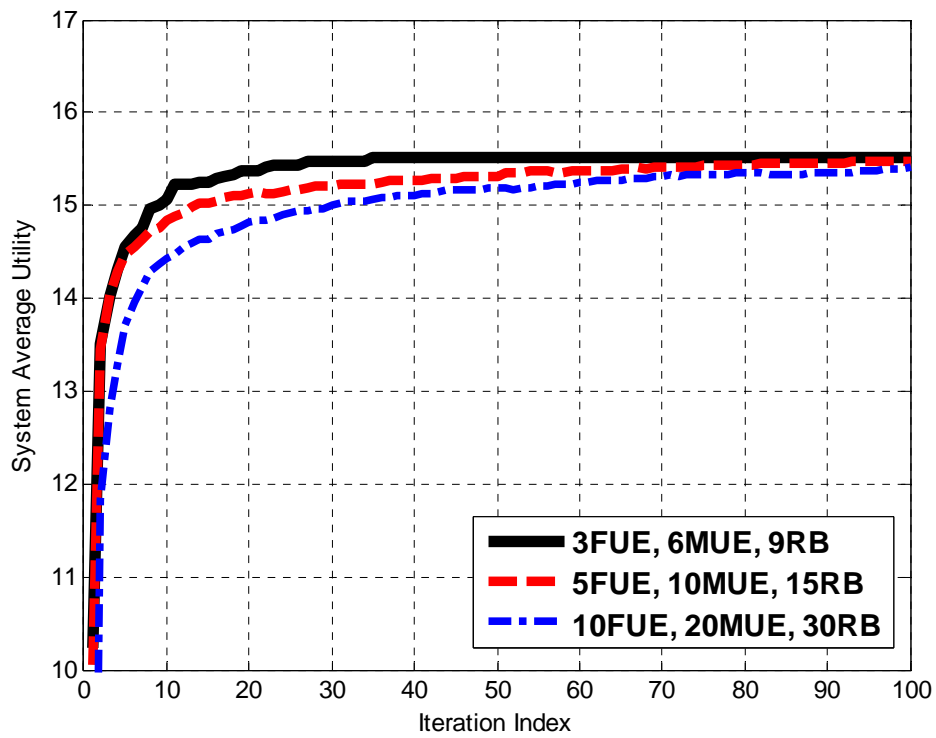
Figure 4.6: Utility comparison between different number of FAPs
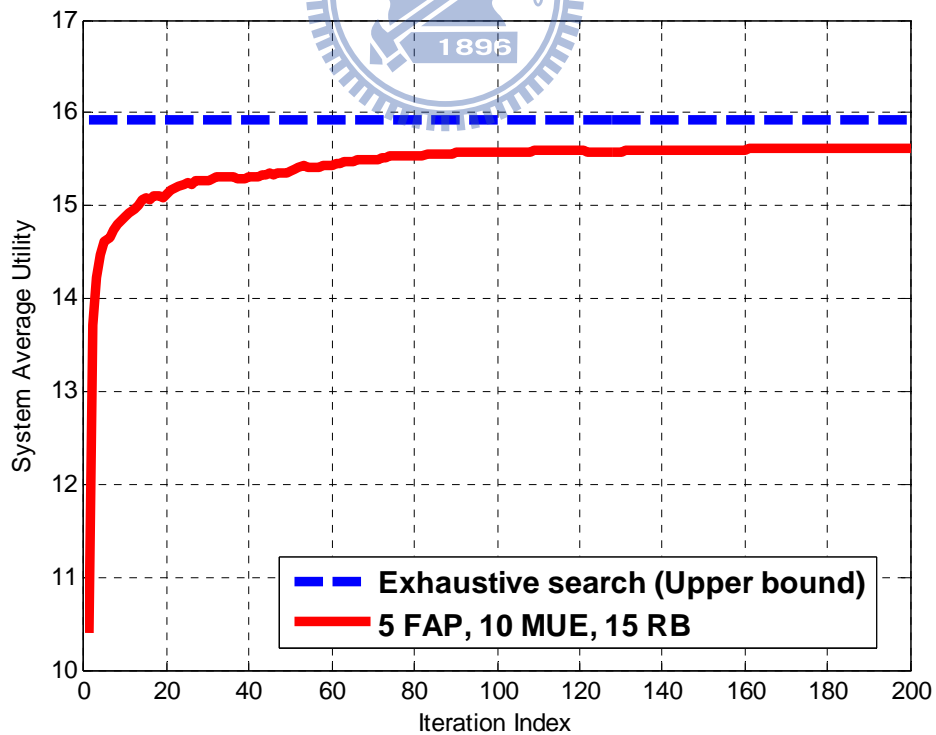
Figure 4.7: Utility comparison between the game-theoretic distributed RB allocation

method and the exhaustive search method

Figure 4.8 shows the problem of insufficient number of RBs. In the case of {5FAP, 10MUE, 13RB}, the number of RBs is not enough and therefore some of FAPs must use the same RB at a time. Therefore, the co-tier interference between FAPs may increase and thus degrade the system average utility.
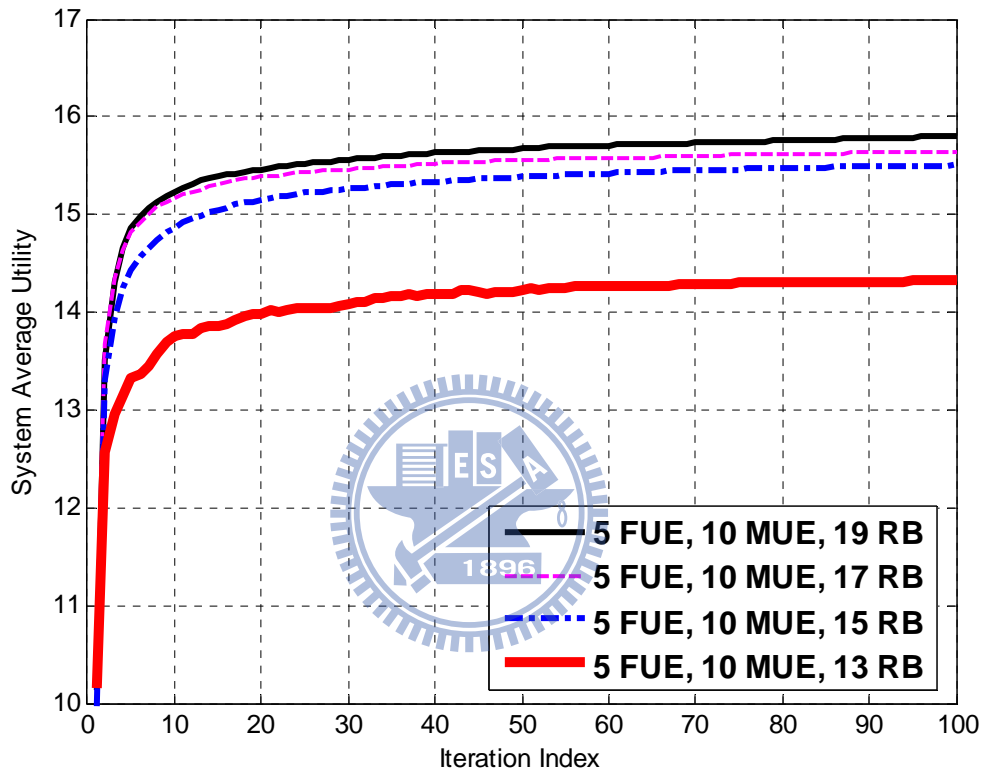
Figure 4.8: Utility with pure overlay spectrum access strategy

To solve the problem of insufficient RBs, we introduce the idea of joint overlay and underlay spectrum access strategy. The basic idea of joint overlay and underlay strategy is to reuse the RBs which have been originally occupied by the FUEs when the number of unoccupied RBs is insufficient. Since some of MUEs are far from FUEs, the cross-tier interference between them is low. Under this situation, we can reuse these RBs on the promise of not introducing unacceptable cross-tier interference to MUEs.

The legend in Figure 4.9 represents the situation that N_{MUE} RBs are firstly occupied by N_{MUE} MUEs, and FAPs can find $N_{aRB} = \left(N_{aRB,1} + N_{aRB,2} \right)$ available RBs with spectrum sensing technique. The result is shown in Figure 4.9, in which the utility does not degrade severely even in the pure underlay spectrum access strategy. Figure 4.10 shows the decreasing of cross-tier interference when the iteration number is increased. This is because FAP will find the best policy to allocate RB with the smallest regret, and the smallest regret also represents the largest utility and the smallest co-tier interference.
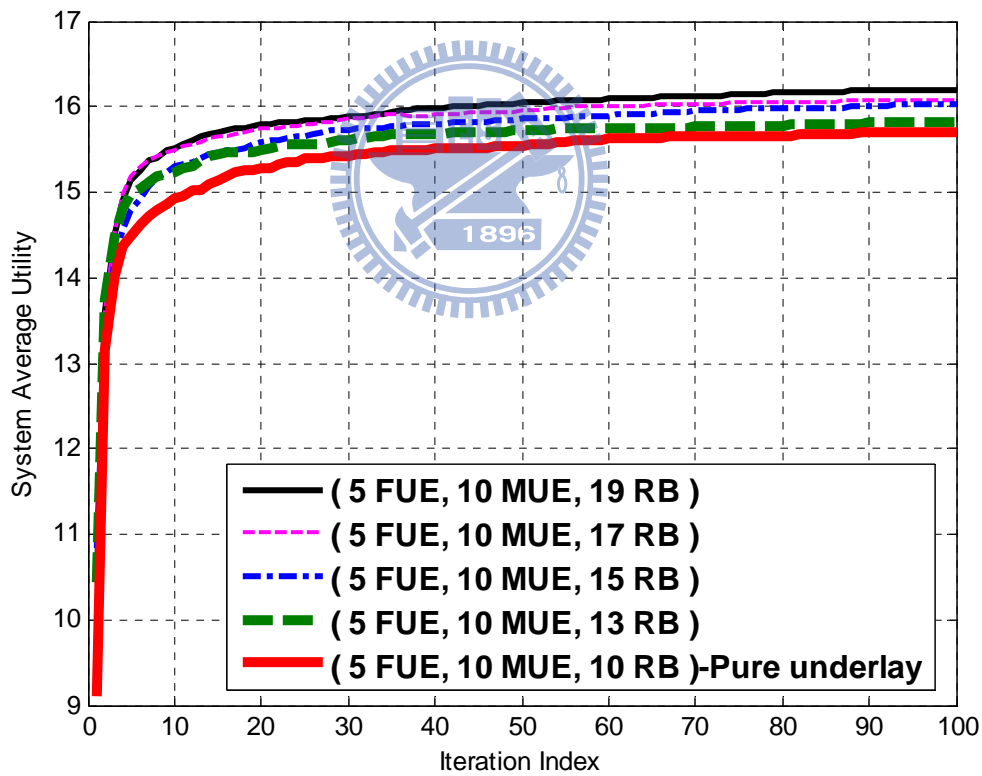
Figure 4.9: Utility with joint overlay and underlay spectrum access strategy
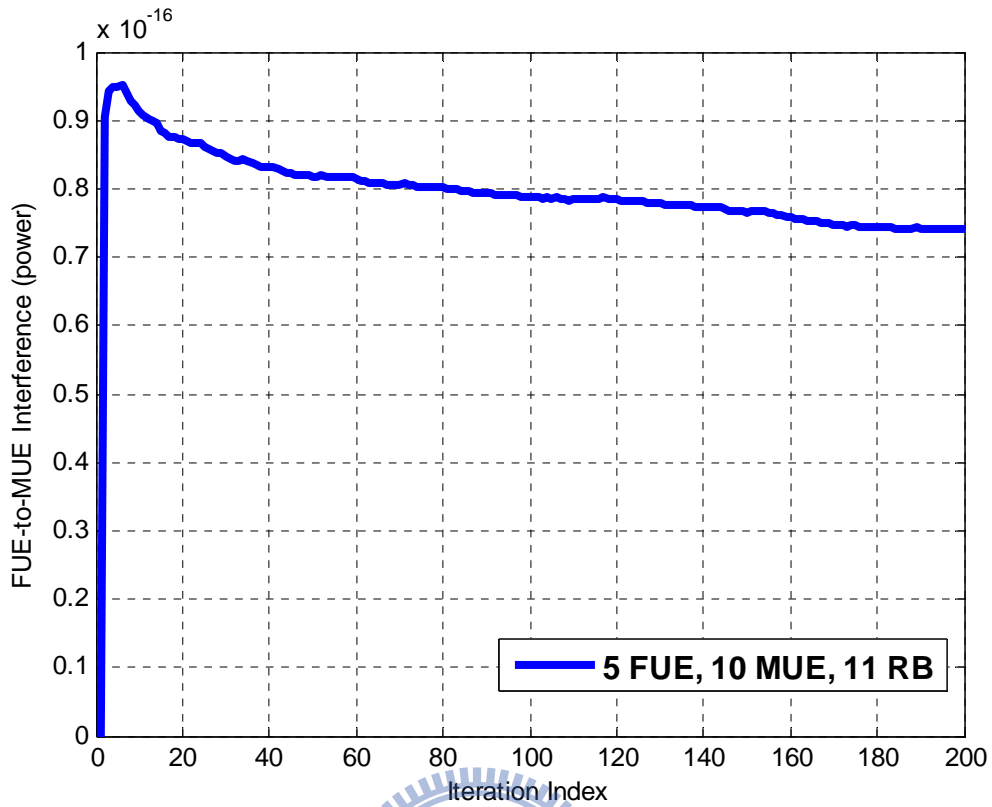
Figure 4.10: Cross-tier interference between MUE and FUE

4.5 Summary

In this chapter, we formulate the RB allocation problem into a non-cooperative game with joint overlay and underlay spectrum access strategy and further employ the regret-matching algorithm to solve it. The computer simulations show that the convergence time varies slightly when the number of FAPs is increased and the regret-matching-based method can approach the global optimum performance after a few iterations. Finally, the proposed method also shows that the frequency reuse factor can be increased with the joint overlay and underlay spectrum access strategy.

Chapter 5

Conclusions and Future Works

In the beginning, we introduce the basic idea of the conventional MME-based cooperative spectrum sensing method and the properties of eigenvalues of covariance matrix. The core concept of MME-based spectrum sensing is to separate the information about the primary signal power and noise power through the EVD function. The maximum eigenvalue composes the information about both primary signal power and noise power; in contrast, the minimum eigenvalue only contains the information about noise power. Therefore, the ratio of maximum and minimum eigenvalues becomes an effective test statistic to determine whether the primary signal exists or not. The MME detection method also performs a blind detection, which detects the existence of primary signal without any knowledge of the signal, channel, and noise power. Consequently, MME detection is a more reliable method under noise uncertainty. However, there still has a problem in the conventional cooperative method. The conventional cooperative method needs to exchange the full information of the received signal, and compute the large covariance matrix with high complexity.

Aiming at reducing the local computational complexity and information exchange overhead in conventional scheme, we propose a new decentralized cooperative spectrum sensing scheme with eigenvalue-based information exchange in cognitive femtocell networks in Chapter 3. In the proposed method, FAPs in the same cluster exchange eigenvalues instead of the entire received signal vector as a metric to build a new test

statistic for spectrum sensing. Besides, we further modify the test statistic by introducing two reliability enhancement techniques to ensure the detection reliability of the proposed scheme and approach the detection performance of the conventional cooperative scheme. The proposed scheme judiciously uses the eigenvalue-based information from neighboring femtocells, and decreases femtocell systems' loading largely. Compared with the conventional cooperative scheme, the proposed scheme exhibits similar detection performance while requiring a much lower overhead and complexity. The computer simulations in Section 3.5 also confirm the effectiveness of the proposed MME-based cooperative spectrum sensing scheme in a femtocell network.

In Chapter 4, we further consider the spectrum access problem based on the sensing information, which we have been discussed in Chapter 2 and Chapter 3. We firstly formulate the spectrum allocation problem into a non-cooperative game with joint overlay and underlay spectrum access strategy and further employ the regret-matching algorithm to solve it. The regret-matching algorithm is a kind of learning algorithm; the basic idea of regret-matching algorithm is to learn about the regret of its actions that had been taken at every time instant and aim at minimizing its regret value. A smaller regret value means that the utility is larger and also means the co-tier interference or cross-tier interference becomes smaller, that is, we can find the best policy to allocate RBs with the smallest interference. The computer simulations in Section 4.4 show that the regret-matching-based method can approach the global optimum performance after a few iterations.

The proposed joint overlay and underlay spectrum access strategy increases the frequency reuse factor effectively. This is because we introduce the spectrum sensing technique to differentiate between the available and unavailable RBs firstly and also reduce the detection uncertainty with a new eigenvalue-based cooperative scheme. Then based on those sensing information, femtocells can find the optimum way, with

regret-matching algorithm, to reuse the RBs on the promise of not causing unacceptable cross-interference to the macro system.

There is still an issue remaining to be further investigated in this thesis. We would like to consider the problem of joint power and spectrum allocation in the underlay spectrum access strategy. Since we only devote our attention to finding the optimum spectrum allocation policy with the smallest interference, we do not consider power control problem in this thesis. If we can design the action space of the game with the power allocation incorporated, the cross-tier interference may be further reduced between the macro and femto networks.
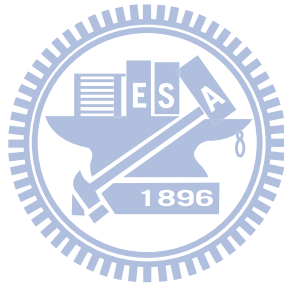
Bibliography

[1]   B. Wang and K. J. R. Liu, "Advances in cognitive radio networks: a survey," *IEEE J. Sel. Topics Signal Process.*, vol. 5, no. 1, pp. 5-23, Feb. 2011.

[2]   S. Al-Rubaye, A. Al-Dulaimi, J. Cosmas, "Cognitive femtocell," *IEEE Veh. Technol. Mag.*, vol. 6, no. 1, pp. 44-51, Mar. 2011.

[3]   "3GPP work items on Self-Organizing Networks," Oct. 2010. Available: http://www.3gpp.org/ftp/Information.

[4]   A. Attar, V. Krishnamurthy, and O. N. Gharehshiran, "Interference management using cognitive base-stations for UMTS LTE," *IEEE Commu. Mag.*, vol. 49, no. 8, pp. 152-159, Aug. 2011.

[5]   P. Xia, V. Chandrasekhar, and J. G. Andrews, "Open vs. Closed Access Femtocells in the Uplink," *IEEE Trans. Wireless Commu..,* vol. 9, no. 12, pp. 3798-3809, Dec. 2010.

[6]   T. Yucek and H. Arslan, "A survey of spectrum sensing algorithms for cognitive radio applications," *IEEE Commun. Surveys Tutss.*, vol. 11, no. 1, pp. 116-130, Mar. 2009.

[7]   Y. Zeng and Y. C. Liang, "Eigenvalue-based spectrum sensing algorithms for cognitive radio," *IEEE Trans. Commun.*, vol. 57, no. 6, pp.1784-1793, June 2009

[8]   R. Tandra and A. Sahai, "Fundamental limits on detection in low SNR under noise uncertainty" *in Proc. IEEE Wireless Networks, Communications and Mobile Computing, 2005 International Conference*, vol.1, pp. 464-469 June 2005.

[9] A. Kortun, T. Ratnarajah, M. Sellathurai, C. Zhong, and C. B. Papadias, "On the performance of eigenvalue based cooperative spectrum sensing for cognitive radio," *IEEE Trans. Commun.*, vol. 5, no. 1, pp.49-55, Feb. 2011.

[10] F. Penna, R. Garello, and M. A. Spirito, "Cooperative spectrum sensing based on the limiting eigenvalue ratio distribution in wishart matrices," *IEEE Trans. Commun.*, vol. 13, no. 7, pp.507-509, June. 2009.

[11] M. Yang, J. An, X. Bu, and L. Sun, "An Improved Eigenvalue-Based Algorithm for Cooperative Spectrum Sensing," *in Proc. IEEE WiCOM'2010*, Oct. 2010.

[12] Z. Quan, S. Cui, and A. Sayed, "Optimal linear cooperation for spectrum sensing in cognitive radio networks," *IEEE J. Sel. Topics Signal Process.*, vol. 2, no. 1, pp. 28–40, Feb. 2008.

[13] J. W. Hung and V. Krishnamurthy, "Cognitive base stations in LTE/3GPP femtocells: a correlated equilibrium game-theoretic approach," *IEEE Trans. Commun.,* vol. 59, no. 12, pp.3485-3493, Dec. 2011.

[14] M. Maskery, V. Krishnamurthy, and Q. Zhao, "Decentralized dynamic spectrum access for cognitive radios cooperative design of a non-cooperative game," *IEEE Trans. Commun*., vol.57, no. 2, pp. 459-469, Feb. 2009.

[15] M. Bennis, and S. M. Perlaza, and M. Debbah, "Learning Coarse Correlated Equilibrium in Two-Tier Wireless Networks", in proc. of the *IEEE Intl. Conference on Communications* (*ICC 2012*), Ottawa, Canada, June, 2012.

[16] N. Nie and C. Comaniciu, "Adaptive channel allocation spectrum etiquette for cognitive radio networks," *in Proc. IEEE 1st DySPAN 2005*, Maryland, USA, Nov. 2005.

[17] S. Hart and A. Mas-Colell, "A simple adaptive procedure leading to correlated equilibrium," *Econometrica*, vol. 68, no. 5, pp. 1127–1150, Sept. 2000.

[18] S. Hart, "Adaptive heuristics: a little rationality goes a long way," *Walras-Bowley Lecture slides*, Sept. 2004. Available: http://www.ma.huji.ac.il/~hart/papers/wb.pdf

[19] L.S Cardoso, M. Debbah, P. Bianchi, and J. Najim, "Cooperative spectrum sensing using random matrix theory," in Proc. *IEEE ISWPC'2008*, pp.334-338, 7-9 May 2008.

[20] I. M. Johnstone, "On the distribution of the largest eigenvalue in principle compomnent analysis," *Annals of Statistics*, vol.29, no.2 pp.295-327, 2001.

[21] D. Cabric, A. Tkachenko, and R.W. Brodersen, "Spectrum Sensing Measurements of Pilot, Energy, and Collaborative Detection on," *in Proc. IEEE 4th MILCOM 2006*, Washington, DC, Oct. 2006.

[22] Z. Liu, H. Zhang, S. Sun, and D. Zhu, "Analysis and improvement of eigenvalue spectrum sensing in cognitive radio networks," *in Proc. IEEE WCSP'2010*, Oct. 2010.

[23] W. S. Lai and T. S. Lee, "A distributed cluster-based self-organizing approach to resource allocation in femtocell networks," *in Proc. IEEE 75th VTC Spring*, Yokohama, Japan, May 2012.

[24] Computational complexity of mathematical operations [Online]. Available: http://en.wikipedia.org/wiki/Computational_complexity_of_mathematical_operation.

[25] H. Yao, Z. Zhou, H. Liu, and L. Zhang, "Optimal power allocation in joint spectrum underlay and overlay cognitive radio networks," *in Proc. IEEE 25th CROWNCOM 2009*, Beijing, China, June 2009.

[26] 3GPP TS 36.814 v9.0.0 (2010-03) "Further advancements for E-UTRA physical layer aspects (Release 9)".

[27] J. R. Smith, *Modern communication Circuits (2e)*, McGraw Hill, 1998, pp. 82.

[28] G. Chouinard, ; Z. D. Lei, W. D. Hu, S. Shellhammer, W. Caldwell, "IEEE 802.22: The first cognitive radio wireless regional area network standard," *IEEE Commu. Mag.*, vol. 47, no. 1, pp. 130-138, Jan. 2009.